Environmental Science Nano

Accepted Manuscript

This article can be cited before page numbers have been issued, to do this please use: F. De Cesare, E. Di Mattia, E. Zussman and A. Macagnano, *Environ. Sci.: Nano*, 2020, DOI: 10.1039/D0EN00268B.

ROYAL SOCIETY OF CHEMISTRY

rsc.li/es-nano

MANUSCRIPT TITLE:

A 3D soil-like nanostructured Fabric for the development of bacterial biofilms for agricultural and environmental uses

CORRESPONDING AUTHOR:
Fabrizio De Cesare
Department for Innovation in Biological, Agro-food and Forest Systems (DIBAF)
University of Tuscia
Via S. Camillo De Lellis - 01100 Viterbo (Italy)
email: *decesare@unitus.it*
ORCID ID: *https://orcid.org/0000-0001-9810-8746*

CO-AUTHORS:
Elena Di Mattia, Eyal Zussman and Antonella Macagnano

JOURNAL:
RSC - ENVIRONMENTAL SCIENCE: NANO

ASSIGNED ASSOCIATE EDITOR:
Prof. Iseult Lynch

MANUSCRIPT:
Full Paper

ENVIRONMENTAL SIGNIFICANCE STATEMENT

Biofilms provide evolutionary benefits to bacteria in ecosystems like efficient nutrient acquisition and resistance to stresses and antimicrobials, and can also be beneficial for some applications. The valuable feature of the 3D nanostructured framework here presented was to mimic the morphology of soil components and the architecture of their spatial arrangement to create a favourable environment for the development of biofilms more similar to those in natural ecosystems, while acting as a carrier of the specific microbial inocula. The additional employment of biodegradable materials will globally result in both more efficient and successful and more eco-friendly and safe products than in traditional uses for applications in agriculture (biostimulants and biopesticides), energy (microbial fuel cells), industry (bioreactors) and environment (bioremediation).

A 3D Soil-Like Nanostructured Fabric For The Development Of Bacterial Biofilms For Agricultural And Environmental Uses

View Article Online
DOI: 10.1039/D0EN00268B

Fabrizio De Cesare[a,b], Elena Di Mattia[c], Eyal Zussman[d] and, Antonella Macagnano[b]

[a]Department for Innovation in Biological, Agro-food and Forest Systems (DIBAF), University of Tuscia, 01100 Viterbo, Italy
[b]Institute of Atmospheric Pollution Research, National Research Council (CNR), 00016 Monterotondo (Rome), Italy
[c]Department of Agriculture and Forest Sciences (DAFNE), University of Tuscia, 01100 Viterbo, Italy
[d]Faculty of Mechanical Engineering, Technion - Israel Institute of Technology, Haifa, 3200003, Israel

KEYWORDS
Bacterial Biofilms, *Burkholderia*, Electrospinning, Nanofibres, Soil, Agriculture, Biostimulants, Biofertilisers, Biopesticides, Environment, Pollutant bioremediation

ABSTRACT

The present study aimed at creating a solid nanostructured scaffold suitable for the development of bacterial biofilms and that enabled bacteria to resist successfully to harsh nutritive and environmental conditions for potential applications. As a model system, we combined a self-standing electrospun nanostructured poly(ε-caprolactone)-based scaffold (*EN-PCLS*) with *Burkholderia terricola* cells. The scaffold structure was fabricated on purpose to include microbeads and nanofibres and mimic the 3D morphological and spatial architecture of soil at the microscale and nanoscale, thus favouring the development of suitable biofilms. The resulting 3D framework displayed an extensive porosity and pore interconnectivity, and a honeycomb wax cell-like arrangement reproducing large cavities in soil. The bacteria firstly deposited a conditioning film onto the *EN-PCLS* to facilitate adhesion. The bacterial attachment was preferentially observed on the nanofibres with cells prevalently oriented along with them, and it persisted until late incubation under stirring, with beads appearing as bacteria-free if deprived of nanofibres on them. Over time, the interaction was improved in terms of stability upon the formation of appendages and release extracellular polymeric substances (EPS). It resulted in more stable adhesion to the nanofibres with enhanced colonisation and the formation of flat bacterial aggregations in the nanofibrous areas inside the honeycomb wax cell-like frames of the *EN-PCLS*. Also, 3D micro- and macrocolonies were formed, hung to nanofibres in between the microbeads of the honeycomb wax cell-like walls. Such microbial organisation evolved into a mature 3D biofilm within 7 d incubation, where bacteria formed densely packed layers of cells embedded into and coated with the EPS matrix that covered the whole *EN-PCLS* like a thick blanket. At the final stage of biofilm development (11 d) both the biofilm and scaffold frameworks appeared partially degraded, the latter being probably utilised as a C-source. Hence, the observed soil-like 3D nanostructured architecture here proposed successfully enabled soil bacteria to develop biofilms on more natural supports than in traditional studies. This strategy seems then promising in creating scaffolds to be used as successful nanobiotechnological carriers for applications in both agriculture (nutrient supply and control of plant diseases) and environment (bioremediation of polluted soils and wastewater).

1. INTRODUCTION

View Article Online
DOI: 10.1039/D0EN00268B

In the '70s, the first pieces of evidence appeared on the prevalent lifestyle of bacteria in ecosystems as attached to surfaces (sessile) and named biofilm, differently from what it was the common belief until then, i.e. that microbes live suspended in the aqueous solutions (planktonic).[1] From that time on, the interactions of bacteria with surfaces have been extensively investigated.[2] However, mobile biofilms can also be formed in the absence of any substratum (flocs and sludge) upon an aggregation of micrometre-size particles.[3] The biofilm development is often related to the possibility for bacteria to survive more successfully in diverse nutritive and environmental conditions and persist for long.[4–7] Bacterial biofilms are formed on a multitude of distinct types of surfaces both natural and artificial, animated and inanimated, including plants, organic residues and soil particles, as well as metals, plastic, glass, rubber, and other materials.[8–10] Bacterial communities have evolutionarily benefited over time from this spatial and mostly functional organisation. However, these benefits for bacteria can result to be either harmful or beneficial for living and abiotic hosts.

The biofilm lifestyle of bacteria has also been demonstrated in the soil in the last decades, prevalently in the volume of soil surrounding the roots (namely, rhizosphere) and at root surface (rhizoplane),[11] where biofilms are involved in microbe-plant interactions and induce beneficial effects like growth stimulation and higher resistance to climate fluctuations and unfavourable environments, as well as to pathogen and pest attacks.[4,5,7,12] Consequently, a great interest has been very recently posed by scientists in the possible utilisation of biofilms to support crop cultivations.[13] Furthermore, the resistance of biofilms has been beneficially exploited within other anthropic contexts concerning the industrial production of biomolecules and energy, and in bioremediation.[14–17] There is a lot of concern by industries and stakeholders in developing novel strategies aimed at favouring the attachment of microbes to surfaces and the formation of biofilms to improve the performances (e.g. rate and efficiency) as well as to overcome criticisms of the production processes where microbes are involved. The environment is another remarkable sector where microorganisms have getting increasing importance. The interest in renewable energy sources has driven to the development of microbial fuel cells, where bacteria tend to develop biofilms around electrodes.[15] At the same time, microorganisms have been extensively used to reduce the contamination of ecosystems by both organic and inorganic pollutants,[16,17] although biofilms have been less studied.[18]

Since biofilms are formed on surfaces upon adhesion, strategies to promote biofilm development have been typically based on both modifications of surface topography and coating depositions aimed at facilitating bacterial adhesion. By the way, a few studies recently demonstrated that specific artificial micro- and nanoscale surface topography motifs are capable of facilitating bacteria attachment more than smooth surfaces.[19,20] However, these articles studied interactions at the early stages, i.e. without observing biofilm formation (with exceptions).[20] Some other articles reported that nanofibres could also act as substrates to grow microorganisms until biofilms for applications in energy production in microbial fuel cells (MFCs) (nanofibrous electrodes)[21] and pollutant removal,[22] but without providing detailed information on the biofilm development. Very recently, some rod-shaped bacteria cells were proven to adhere preferentially to nanofibres both with size slightly[23] and much smaller[24] than the bacterial cell diameter, and aligned along with them once the fibres had been previously coated with a conditioning film released by the cells.[24]

Microorganisms have also been recently started to be included in some agricultural products (biostimulants, biofertilisers and biopesticides) to reduce the impact of agrochemicals on the environment and health.[25–27] Similarly, in the last decades, microorganisms have been employed to remove contaminants from wastewater and soil through bioremediation treatments.[28] However, in both agriculture and bioremediation, the microbe-based inocula commercially available to date to support crop yields (typically plant growth-promoting rhizobacteria - PGPR) or degrade pollutants often result ineffective in playing their actions, especially as concerns non-sporulating species.[29] The microbes added to soils, in effect, have to face several adverse conditions (e.g. harsh environment, nutrient limitation and competition with other organisms) towards which resident microbial populations are usually more adapted. Hence, there is an increasing demand

for novel, more efficient and effective products for both agricultural and environmental applications.

The present study, then, aimed at creating solid nanostructured carriers suitable for the development of bacterial biofilms for applications in both agriculture (e.g. nutrient supply and control of plant diseases) and environment (bioremediation of polluted soils and wastewater). Specifically, the 3D nanostructured scaffolds to create were intended to mimic the soil architecture (Fig. 1). The morphological spatial distribution of soil components was considered as a major model feature of soil. Soil is a very complex material, and such complexity derives both from a variety of components with different shapes but mostly from a multitude of chemically different compounds. However, it has been demonstrated that in the adhesion of bacteria to surfaces the specific chemistry of surfaces can often be irrelevant, because of the coverage of materials with organic coatings (conditioning films) released by bacteria or present in the media.[24,30] Conditioning films can remarkably alter the physical, chemical and physicochemical properties of the surfaces. The topography of surfaces has been demonstrated to be of pivotal importance in the adhesion of bacteria.[20,24] Bacteria have been proven to be capable of accurately sensing the morphology of the surfaces so that they prefer the interaction with fibres with nanosized diameter[24,31] or can repel the adhesion to surfaces with some specific topography.[32] In soil ecosystems, in effect, it is rare to find broad flat surfaces similar to the artificial ones aforementioned. Soil consists of solid particles alternated with voids and fibrous organic matter. Hence, it is presumable that soil bacteria might feel as unnatural the flat surfaces typically used for studying biofilm formation in biomedical (e.g. implants), water (e.g. pipes), energy (MFCs), industrial and remediation applications (metals and alloys, glass, silicon, organic polymers),[18,33,34] although they can adhere to them. Consequently, bacteria coming across flat surfaces might express unnatural and then less effective and efficient behaviours suitable for agricultural and environmental applications, possibly inducing also misinterpretations. On the contrary, we believe that in more natural environments such as soil-mimicking surfaces, bacteria would express more probably and successfully the phenotypic traits typical of the telluric species and would develop more natural and efficient biofilms.

We intended to create 3D nanostructured scaffolds mimicking the soil architecture by using electrospinning technology. Electrospinning is a versatile technology generating fibres when polymer solutions stored in syringe-like containers are driven out under an electric field.[35] Fibres can be produced in a range of diameters from nano- to micro-scale and with a variety of morphologies and arrangements from scattered nanofibres, 2D nanofibrous thin layers and 3D nanofibrous scaffolds.[36–38] Electrospun nanofibrous materials have been used in the last decades in several applications.[39–43] Polymer solutions under an electric field can also produce droplets or beads when low viscoelasticity is employed (electrospraying).[44–46]

In the present study, non-toxic polymers were preferred to prevent possible inhibitions of bacterial growth until mature biofilm formation of the selected species, but also to obtain safe and low-impact fabrics to be used in target applications such as agriculture and environment). We selected the poly(ε-caprolactone) (PCL), an aliphatic polyester polymer, because of its biodegradability, biocompatibility and hydrophobicity, which have recently made it widely used in medical applications.[47] Additionally, PCL nanofibrous scaffolds have been extensively employed in medicine for the capacity of this polymer to support the growth of a variety of human cell types for tissue engineering (fibroblasts, chondrocytes, and osteoblasts)[48–50] and more recently they have been demonstrated favouring the adhesion and proliferation of bacterial cells without any apparent growth inhibition.[24]

The bacterial species employed in this study as a model species was *B. terricola*. *Burkholderia* is a proteobacteria genus that is of great interest because including species that are almost ubiquitary in natural terrestrial ecosystems while other species are pathogens for humans, plants and animals, thus causing possible opposite effects, from beneficial to harmful.[51,52] *Burkholderia* spp. was selected because supposed to match the requirements necessary to achieve the targets of this study. The genus *Burkholderia* spp. is widely distributed in soils and has been proven to have

remarkable biotechnological potential in the decontamination of polluted soils.[53] In detail, *B. terricola* is a species typically present in the rhizosphere (the volume of soil surrounding the plant roots) of a variety of plant species, where it acts as a PGPR.[54,55]
Hence, this study was aimed at creating an artificial electrospun fabric characterised by a 3D arrangement of granular particles, fibres and fibrous frameworks, and high porosity (voids, single and interconnected pores, and channels) enabling gaseous (air and VOCs) and liquid (nutrients and wastes) inward and outward fluxes, thus tentatively reproducing the spatial architecture of natural soils. Therefore, the creation of a beads-and-fibre Electrospun Nanostructured PCL Scaffold (*EN-PCLS*) was hypothesised to match the desired requirements of a soil-like matrix possibly recognised by selected soil bacteria at micro- and nanosize level as a more "comfortable" and "familiar" environment for living and less toxic than other plastic structures.[56,57] The *EN-PCLS* here created were then inoculated with *B. terricola* cells. The various phases of biofilm development from bacterial adhesion to biofilm formation and degradation were then followed and investigated and the possible applications of the resulting nanobiotechnological products were evaluated.

2. MATERIALS AND METHODS

2.1. Chemicals and reagents

Poly(ε-caprolactone) (MW 45 kD), chloroform ($CHCl_3$) and ethanol (C_2H_5OH) were purchased from Sigma-Aldrich and used without further purification. All bacteriological reagents and 2-(4-iodophenyl)-3-(4-nitrophenyl)-5-phenyl-2H-tetrazolium chloride (INT) were also purchased from Sigma-Aldrich.

2.2. Nanostructured scaffold fabrication

PCL concentrations of 10.7% and 11.7% (w/w) (PCL_1 and PCL_2 respectively) were dissolved in 4:1 (v/v) $CHCl_3$:C_2H_5OH ratio solution and a mixture of beads and nanofibres were deposited by electrospinning over an aluminium foil to form a beads-and-fibres framework mimicking the soil architecture and the morphologies of the solid components of soil at the micro- and nanoscale. Chloroform was used as the main solvent while ethanol, a non-solvent, was added due to its higher boiling point (78°C) and high dielectric constant (ε=25) to reduce the high-volatility of chloroform at the droplet-air interface and prevent polymer clogging in the syringe during the process, while favouring the formation of both beads and fibres during the process.[58,59] The electrospinning machine here employed was fabricated in CNR-IIA-Rome (Italy). It consisted of a high voltage oscillator (100 V) driving a high voltage (ranging from 1 to 50 kV), a high power AC-DC (alternative current-direct current) converter, a syringe pump (Model KDS 200, KD Scientific) and a clockwise rotating conductive disk collector with a diameter of 12 cm. Scaffolds composed of beads and fibres (*EN-PCLS*) were obtained by applying 4.9 kV of electrostatic DC voltage between the tip of 5 cm long stainless steel of a syringe housed in a syringe pump (950 $\mu L\ h^{-1}$ in feed rate) and an aluminium foil housed on the grounded collector set at 7 cm working distance and perpendicular to the syringe pump. The depositions were carried out in a home-made clean box equipped with temperature and humidity sensors. The deposition time was fixed at 5 h, in order to obtain proper coverage of the deposition platform and a suitable thickness of the material to manipulate. The rotation speed was set to 400 rpm, and depositions were carried out at about 24°C and 30% RH (relative humidity). To prevent possible microbial contaminations during the electrospinning procedure and the following incubation of *EN-PCLS* with the bacteria strain of interest, all the surfaces of the deposition box and the electrospinning machine were sterilised with disinfectants, and any tool for handling was autoclaved or flame sterilised, or both prior to use.

2.3. Nanostructured scaffold morphological characterisation

2.3.1. Imaging

The various beads-and-fibres *EN-PCLS* obtained by electrospinning were analysed through various image capturing instruments (stereomicroscope, optical microscope, SEM and TEM) to observe their morphological features at macro-, micro- and nano-scale. The pristine *EN-PCLS* as well as those incubated with the culture medium and without bacteria (control) were sampled under sterile conditions and analysed after rinsing with sterile deionised water. Differently, to capture images of *EN-PCLS* retaining bacteria cells during the various phases from adhesion to biofilm development, *EN-PCLS* were collected from the batch cultures after 3 h, 5 h, 20 h, 28 h, 48 h, 7 d and 11 d of incubation (§2.4.2). All *EN-PCLS* after sampling were washed in sterile deionised water to remove any material unspecifically bound to the *EN-PCLS*, both animate and inanimate. Samples were then variously processed based on either the test or the optical technique used and depending on the presence or absence of bacteria.

2.3.1.1. Light microscopy

Semi-thin sections (1 μm) of the nanostructured PCL scaffolds were collected and placed onto slides, stained by Toluidine Blu and observed at a Zeiss (Axiophot) microscope equipped with a colour video camera (Axio Cam MRC) using a computer-assisted image analysis system (AxioVision).

2.3.1.2. Electron microscopy

The variously treated *EN-PCLS*, regardless of their incubation with bacteria, were prepared for Scanning Electron Microscopy (SEM) and Transmission Electron Microscopy (TEM) investigations as follows.

For SEM analyses, after initial washing upon sampling, specimens were pre-fixed for 30 min at 4°C with 2.5% (v/v) glutaraldehyde in cacodylate buffer 0.1 M pH 7.2 containing 0.075% (w/v) ruthenium red and 0.075 M lysine acetate. After 3x10 min of washing at 4°C in the same buffer, samples were fixed with 2.5% glutaraldehyde in 0.1 M cacodylate buffer pH 7.2 for 2 h at 4°C. After further rinsing, as described hereinbefore, samples were post-fixed with 2% (v/v) osmium tetroxide in cacodylate buffer for 2 h at 4°C. Specimens were washed 3x15 min at 4°C in the same buffer and dehydrated in a graded ethanol series. Samples were dried by the critical point method using CO_2 in a Balzers Union CPD 020. Samples were then attached to aluminium stubs with carbon tape and observed by a JEOL JSM 6010LA electron microscope after a gold sputter-coating in a Balzers MED 010 unit.

For TEM observations, specimens upon sampling and washing firstly underwent fixation and dehydration, similarly to SEM samples, and then infiltration with mixtures of LRWhite resin/ethanol in different percentages. At the end of the procedure, samples were embedded in LRWhite resin, 2 days at 50°C. Blocks were cut with a Reichert Ultracut ultramicrotome equipped with a diamond knife, and ultra-thin sections (60-80 nm) were collected on copper grids, stained with uranyl acetate and lead citrate, and observed with a JEOL 1200 EX II electron microscope. Micrographs were captured by the Olympus SIS VELETA CCD camera equipped with iTEM software.

2.3.2. Size distribution of beads and fibres

The measurement of the average diameter of beads and fibres was calculated based on images captured by SEM, as follows. The SEM images were processed by Gwyddion© 2.3 software (GNU General Public License)[60] to calculate the grain and fibre size. Image analyses were carried out on global amounts of 220 beads and 145 fibres. Similarly, honeycomb cavities mean diameters were calculated onto 135 and 150 areas of the wet and dry samples, respectively. The Normal probability distributions (known as Gaussian or bell-shaped curve) based on the mean and the standard deviation and representing the density function of the grain size were calculated using Microsoft Excel©.

2.3.3. Contact angle

The contact angle of the two types of fabrics (*EN-PCLS$_1$* and *EN-PCLS$_2$*) was measured as follows. Pictures of water drops (8 µl and 7 µl, respectively) upon deposition on the nanostructured fabrics by dripping from a micropipette were captured by a USB-Digital Microscope (2.0 MPx, DIGIMICROSCOPE) in 10 s. The water contact angle (WCA) values were measured by the LBADSA method[61] running within DropSnake©, a plugin implemented for ImageJ software.[62]

2.3.4. Porosity

The global porosity of *EN-PCLS$_2$* was measured based on the liquid intrusion method as follows.[63] Briefly, about 1 cm^2 pieces of the nanostructured scaffolds were weighed and then soaked into absolute ethanol for 10 min and then weighed again. The weight of both dry and soaked samples was measured and then converted into PCL and ethanol volumes based on the density of the two substances. Finally, global porosity was calculated as per cent of volume of ethanol relative to the total volume of the nanofabrics. The procedure was carried out in four replicates (*n=4*).

2.4. Biofilm development

2.4.1. Inoculum preparation

Bacterial cells of *Burkholderia* strain IF25 were isolated from a vineyard soil and preliminary assigned to *Burkholderia terricola*.[54] The bacterial inoculum in each independent experiment was set up as follows: the original culture was grown at 30°C in Luria-Bertani (LB) broth and maintained at 4°C on LB agar plates.[64] *B. terricola* IF25 cells were pre-cultured (30 ml suspension) in the conditions aforementioned before being incubated with *EN-PCLS*.

2.4.2. Biofilm development

Two independent experiments were performed to assess the formation of biofilm on the *EN-PCLS*. In each experimental trial, the various stages of biofilm formation from reversible adhesion, irreversible attachment, biofilm maturation and degradation were assessed in batch cultures (glass Erlenmeyer flasks) containing 25 ml of glucose mineral broth (GMB), as medium, consisting of (g L^{-1}): 2.2 g L^{-1} Na_2HPO_4; 1.4 KH_2PO_4; 0.6 $MgSO_4 \cdot 7H_2O$; 3.0 NH_4SO_4; 2.0 glucose and trace element solution.[65] *B. terricola* IF25 pre-cultured cells were inoculated in the GMB medium at 2% (v/v final concentration) to give 1.2 ± 0.3 x 10^6 CFU ml^{-1}, and 1 cm^2 *EN-PCLS* deposited onto the aluminium were finally added. Bacteria in the flasks were grown aerobically in the dark (on an orbital shaker at 80 rpm) at 30°C. Trials were arranged in a completely randomised block design with independent sampling at fixed times. Specifically, four batch cultures (in each trial) were created at T_0 by adding 48 pieces of *EN-PCLS*, deposited onto aluminium foil, to four flasks (12 pieces each). Bacteria-colonised *EN-PCLS* samples were collected after 3 h, 5 h, 20 h, 28 h, 48 h, 7 d and 11 d of incubation (i.e. corresponding to exponential and early and more extended stationary phase of cells growth), depending on the analyses to carry out. A separate set of flasks was used as a control without bacteria (*CEN-PCLS*). The *EN-PCLS* with or without immobilised bacteria were washed in sterile deionised water upon sampling and then further processed or tested.

2.4.3. Vital and metabolically active bacteria cells

Cell integrity and metabolic activity have been often measured using tetrazolium salts. Among them, 2-(4-iodophenyl)-3-(4-nitrophenyl)-5-phenyl-2H-tetrazolium chloride (INT) is one of the most widely used tetrazolium salts for assessing microbial viability,[66] although some toxic effects have been sometimes observed.[67] Based on its features, INT was used to measure both cell integrity and metabolic activity of immobilised bacteria onto *EN-PCLS* as a consequence of the reduction of this tetrazolium salt by the dehydrogenase activity which is part of the bacterial

respiration process, with the formation of the relative formazan that is accumulated intracellularly. Briefly, to test the bacterial vitality during the biofilm development and persistence (§2.4.2), bacteria-colonised *EN-PCLS* samples were collected from distinct batch microbial cultures sampled at 5 h, 20 h, 28 h, 48 h, 7 d and 11 d incubation periods, then washed in sterile deionised water and placed in flasks containing INT solution (0.01% w/v of redox indicator in 0.1 M phosphate buffer, pH 6.8, and LB 1:20 v/v final dilution). Control samples (*CEN-PCLS*) were collected from a separate set of flasks without bacteria. Bacteria-colonised *EN-PCLS* were then incubated in the dark for 4 h at 30°C, for the colour development, and they were finally treated with absolute alcohol, after having been washed and dried, for the formazan extraction.[68] The resulting solutions after filtration were measured for absorbance at 495 nm by a spectrophotometer. The means and the standard deviations based on four replicates per sample (n=4) expressed as absorbance values normalised to the standard size of the *EN-PCLS* (namely 1 mm^2) were calculated using Microsoft Excel.

3. RESULTS AND DISCUSSION

Soil consists of little solid particles alternated with voids (pores and tunnels) periodically filled with air and water or both of them. The solid particles mostly interacting with microorganisms (fine fraction) are mineral particles and organic fragments in a broad range of dimensions (Fig. 1). The mineral particles in the range 2-50 µm (mostly silt and clay, based on USDA or IUSS classifications)[69] usually present platy, spherical and tubular morphologies and are more attractive for microbial populations because they are more capable of retaining water and nutrients.[70] Even the fresh organic tissues, especially those reduced to little fragments, are densely colonised by microorganisms (bacteria, fungi and actinobacteria) that degrade and transform them into materials (also known with the old terminology of humic substances) displaying spongy, globular, fibrous or nanotube-shaped, and reticulated morphologies, sometimes forming fishnet-like porous membranes.[71,72] These membranes, in the last decades, have been suggested resulting from the self-assemblage and supramolecular association of organic compounds into well-ordered structures.[71] These solid inorganic and organic particles and fibrous materials are typically arranged in healthy natural soils in aggregates with dimensions from < 250 µm (microaggregates) to > 250 µm (macroaggregates) to form a porous structure,[73] where pores range from < 0.1 µm (Cryptopores) to 0.1-5 µm (Ultramicropores), to 5-30 µm (Micropores), to 30-80 µm (Mesopores), and to > 80 µm (Macropores), and micropores and mesopores are those assigned to host the most of microbes present in soils.[74] Hence, the soil architecture at the micro- and nanoscale level, i.e. at which microbes interact with the abiotic soil mineral and organic components, seems to be composed of inanimate structures with mostly globular and fibrous (as both single fibres and networks) morphologies and void spaces or pores with various sizes. Recently, Otten and collaborators developed 3D-printed Nylon 12 macrostructures based on tomography analyses of soil sections and reproducing the soil architecture.[56,57] However, these constructions were composed of plastic materials suitable for laboratory studies but environmentally incompatible with applications in natural ecosystems. Furthermore, these artificial arrangements did not also resemble the soil configuration at both the micro- and nanoscale level, since providing a spatial resolution of 30 µm, i.e. much greater than microbial size.[56] On the contrary, in the electrospun nanostructured soil-like scaffolds here created, soil bacteria cells were expected to attach, settle and proliferate, following their natural behaviours and attitudes based on the phenotypic traits typical of the species selected (*B. terricola*), until forming proper and more natural biofilms.

3.1. Nanostructured matrix

Some mixtures of polymers and solvents were tested in the electrospinning processing to create 3D nanostructured frames mimicking the soil architecture to achieve the target aforementioned. The electrospinning process was tuned on purpose to generate suitable beads-and-fibres scaffolds.

However, only some of the polymers tested fulfilled the requirements necessary for the creation of 3D frameworks satisfactorily similar to soil, especially as concerns the formation of proper beads of various size separate from the fibres, and with sufficient mechanical stability capable of sustaining the stirring applied during the incubation with bacteria. PCL resulted in being the right candidate for achieving the goal fixed, as also demonstrated by the study of Ahirwal et al. (2013).[75] We tested several PCL dissolving solvents with to reduce the environmental impact of the electrospinning process, i.e. the use of toxic organic solvents. Unfortunately, only $CHCl_3$ mixed with C_2H_5OH successfully provided soil-like frameworks matching the expectations. Incidentally, to prevent possible harmful effects on the bacterial cells caused by the solvents with consequent inhibition of adhesion and proliferation of the bacterial population, solvents were extensively removed from the *EN-PCLS* under a fume hood. Fibres are the typical products of the electrospinning process. Still, beads can also be generated, although they are commonly considered as "by-products" or structural defects of the electrospinning process. Bead formation is then commonly prevented by tuning the electrospinning parameters such as polymer concentration and the type of solvent used[76] that can affect both the viscosity of the solution and the surface tension because of the electrical forces breaking the electrospinning jets.[35,45] Low polymer concentrations usually form spindle-like or spherical (rarely or on purpose) beads[77,78] but beads alone can also be produced.[79] Even bead size values and distribution can be tuned based on the procedure performed.[76,79] Hence, by adjusting the deposition parameters, electrospraying can be turned into electrospinning so that the deposited materials can turned from beads alone into beads and fibres, until fibres alone populations.
In this study, we obtained two types of beads-and-fibres scaffolds, by tuning the parameters of the electrospinning deposition on aluminium foils and the concentration of PCL in $CHCl_3/C_2H_5OH$, named *EN-PCLS$_1$* and *EN-PCLS$_2$*, mostly differing in the PCL concentration (10.7% w/w and 11.7% w/w, respectively) and resembling enough the soil morphology and architecture aforementioned.

3.1.1. Nanostructured scaffold morphological characterisation

3.1.1.1. Optical microscope analyses

Optical investigations of the overall macroscopic upward growth of the two 3D mats showed they looked like tufted carpets (Figs. 2a and 3a), where *EN-PCLS$_1$* displayed a thick and more complex architecture (about 1.8 mm wide), while *EN-PCLS$_2$* exhibited a thin structure (about 1 mm wide) (Figs. 2 and 3). In more details, *EN-PCLS$_1$* exhibited about 1.4 mm tall tufts composed of pinnacle- and flake-shaped protrusions (Figs. 2b,c,e,f), while *EN-PCLS$_2$* showed simpler circular crests (Figs. 3b,c). Optical microscope pictures of cross-sections of the pristine *EN-PCLS$_2$* confirmed the presence of both beads and fibres in the electrospun frameworks. Additionally, beads appeared either grouped into irregular aggregates separate from the fibres or as distributed along chains (Fig. 3d), but in this case, they mostly appeared as partially fused (Fig. 3d, red arrows) and not crossed by fibres, like in the case of beaded fibres, also known as beads-on-a-string fibres (Fig. 3d).[35,45] Even when linked to fibres, in effect, beads appeared as deposited on them or oppositely the fibres appeared laying on the particle surfaces and not crossing them (Fig. 3d, light blue arrows), as it happens when beads are usually originated from the same jet of the fibres and have spindle-like shapes with aspect ratios > 1. Here, instead, the beads displayed aspect ratios ~ 1 (Fig. 3d).

3.1.1.2. Electron microscope analyses

BEADS-AND-FIBRES FRAMEWORKS

The SEM investigations of the self-assembled micro- and nanostructures in both the matrices confirmed the presence of beads and fibres. The analyses of the dimensional distribution of both pristine beads and fibres in *EN-PCLS$_2$* showed that the diameters of the particles ranged within 0.34-12.43 μm, with a mean diameter as large as 6.1±3.6 μm and 7.6 μm median value (Figs. 4a),

while the size of the fibres ranged from 10 nm to 170 nm, with 75.1±33.8 nm mean diameter and 77.0 nm median values (Figs. 4b). In *EN-PCLS$_1$*, instead, the average particle size was slightly larger, though it was difficult to measure them because the beads quite always appeared fused (Fig. 2e inset). In any case, the particles of both the pristine nanostructures displayed an aspect ratio ~1 so that they could be reasonably classified as microbeads or microspheres. At the same time, fibres were assigned to nanofibres, based on the standard definition of nanomaterials (i.e. ≤100 nm in at least one of the three spatial dimensions).[80]

Moreover, it is worth noting that, regardless of the type of *EN-PCLS*, the microbeads displayed a very smooth surface, as compared with those generated by the electrospray, often appearing as lumpy (Fig. 3f).[79] Furthermore, SEM micrographs of *EN-PCLS$_1$* showed that, in the fabric volumes, microparticles were the prevalent component, relative to nanofibres, especially in the protruding structures, thus resulting in more compact structures (Fig. 2c,e), while the spaces in between these protuberances were dominated by the nanofibres (Fig. 2e, yellow arrows). Differently, in the global volume of *EN-PCLS$_2$*, a prevalence of nanofibres over microbeads was observed (Fig. 3c, yellow arrows). The difference in the number of microbeads vs nanofibres observed in the two *EN-PCLS* could be reasonably ascribed to the diversity in the polymer concentration of the two solutions before electrospinning (10.7% vs 11.7% w/w). Other studies on PCL and other polymers demonstrated that the increase in polymer concentration reduces the number of beads in favour of fibres.[75,81,82]

HONEYCOMB-LIKE PATTERNS

Interestingly, both the *EN-PCLS* in top views displayed a sort of repetition of holes or cavities at the surface of the overall structure surrounded by walls, resembling the architecture of wax cells in a bee honeycomb (Figs. 2a,d; Figs. 3a,b). Electrospun nanofibres have been reported to self-assemble into honeycomb-patterned nanofibres also on non-patterned substrates as a result of the balance between simultaneous attractive and repulsive electrostatic forces.[75,82] Here, *EN-PCLS$_1$* did not show at first instance a similar pattern in the prevalently thick areas because of the tall protuberances (Fig. 2d), but in the thinner rarer portions of these samples such organisation was more evident (Fig. 2c). In *EN-PCLS$_2$*, the honeycomb-like pattern was visible at the various magnifications (Figs. 3a,b,c,e). In honeycomb structures, the wax cell-like cavities or pores at the surface of fabrics can display various regular and irregular shapes, depending on the polymers and the electrospinning conditions.[75,81,82] The size of these cavities can also be influenced by polymer concentration and time of deposition[75] and working distance.[82] In our study, we observed that the cavities in the pristine electrospun fabrics showed a wide diameter distribution that in *EN-PCLS$_2$* ranged from 97 μm to 582 μm and a mean value as large as 328±104 μm, and a surface area in the range 7.39-265.44 10^3 μm^2, with about 92.8±57.5 10^3 μm^2 mean value, i.e. in agreement apparently with the values and the relative trends reported in other studies.[82] However, it is worth noting that the honeycomb structure of *EN-PCLS$_2$* was modified once incubated for 3 h with the medium containing bacteria. The cavities, in fact, displayed an average diameter as large as 61±18 μm and in the range 23-111 μm (Figs. 4c), and a surface area about 3.17±1.80 10^3 μm^2 mean value within a range 0.43-9.68 10^3 μm^2, then resulting in a remarkable decrease (-81% and -97% in the average diameter and surface area, respectively). Notably, since such difference in the cavity diameters was much larger than around 30 nm, because of the conditioning film deposition (2x15 nm thickness) on the various materials of the frameworks, the diameter reduction was maybe due to a shrinkage of the whole nanostructure fabrics during the incubation and not to the mere contribution of the coating.

Honeycomb structures in electrospun materials were observed for the first time by Deitzel et al. (2001).[81] This arrangement has been explained as mostly due to heterogeneous depositions leading to the generation of thick domains on the collectors surface[75] that barely discharge relative to the initial phases of the electrospinning deposition. Such thick domains can be originated by different causes. They would induce the accumulation of electrostatic charges on these self-organised aggregates and the repulsion of the incoming charged electrospun fibres, thus

preventing them to be deposited on the collectors and to dry and eventually form the 3D honeycomb patterns following a three-branched organisation with an intersecting angle of 120°.[81] In the honeycomb-like patterned *EN-PCLS* here created, especially in *EN-PCLS*$_2$, the self-assembling structure was maybe generated by fibres and beads that acted as thin and thick domains,[75,83] instead of creating a proper bi- or multimodal distribution of fibres in multiple populations with diverse size diameter.[75,83,84] Incidentally, in most of the articles on electrospun honeycomb structures where both fibres and beads are present, beaded fibres were observed as element comprising these self-organised 3D patterns,[75,81] where beads were linked by fibres and distributed like in a rosary chain. In the present study, a multitude of microspheres (aspect ratio ~ 1) and a much higher number of thin nanofibres were produced in *EN-PCLS*$_2$, and the occurrence of beaded nanofibres was not evident, primarily because of the significant difference between the size of nanofibres and that of beads (~ 75 nm mean value - Fig. 4b - vs ~ 6.1 µm mean value - Fig. 4a, respectively). Such evidence made difficult the identification of the spheres as part of the fibres (i.e. crossed by the nanofibres) or disposed along single nanofibres, as in the studies aforementioned.[75,81]

Additionally, microbeads appeared preferentially located in the walls of the patterned structures, while thin nanofibres were deposited both in the walls, together with the microparticles, and in the honeycomb cell-like cavities, as the prevalent component (Fig. 3c). In other studies, a similar distribution was also observed, but spindle-like beads (< beads-to-fibres size ratios) in the cavities were more numerous maybe because beads were not physically separated from the nanofibres (beaded fibres).[75,81] Two possible motives to explain the results in our study might be that, in the first case, microbeads driven by electrostatic repulsion towards the walls of the honeycomb during the electrospinning deposition could stretch the nanofibres to which they were linked because of the very high beads-to-fibres size ratios here calculated (~ 80) and then of the much higher weight of the microbeads relative to the nanofibres so that only nanofibres would remain between the walls. The second possible reason of the remarkable different distribution between microparticles and nanofibres might be that, because of the typical electrospinning conditions here fixed, two independent populations of microparticles and nanofibres were produced that segregated occupying the cavity walls (microbeads) and the space in between (nanofibres).

Interestingly, it was demonstrated that when two independent populations of beads and fibres were co-deposited by electrospraying and electrospinning, respectively, the two types of elements successfully self-assembled into honeycomb-like structures because of the local variations of the electric field acting as the driving force of this arrangement.[83,84] Consequently, the microparticles appeared as segregated into the honeycomb cell walls, while only stretched fibres were present in the interspaces between the walls,[83,84] alike to our findings. The similarity between Fig. 3e and the figures in these two articles seems to support the hypothesis of two separate populations of microbeads and nanofibres, instead of beaded nanofibres, comprising the honeycomb-like arrangements. However, except for when distinct populations of beads and fibres are produced on purpose, it is still unclear, also in very recent publications, to identify if beads and fibres comprising honeycomb-like arrangements produced through a single electrospinning process are present as two independent populations or are beaded fibres.[82]

The resulting honeycomb-like architecture composed of beads and fibres displayed many features potentially suitable to accomplish the specific aims of this study (i.e. the development of a microbial biofilm in a soil-like structure) such as the large surface area and the elevated porosity of the framework, in comparison with the typical flat nanofibrous structures present in the literature.[85,86] In addition, the honeycomb-like pattern has been recently described as present in the structure of humic substances comprising the soil organic matter.[71,87] This observation has been linked to the new theories on the nature of humic substances as combinations of supramolecular associations, micelles and retained biomolecular fragments.[88,89] Based on these findings, the presence of honeycomb-like patterns in the soil-like 3D frames created in this study further enforces the similarity of the created artificial nanoframeworks with the soil structure, and

then of the goodness of the approach proposed in this study and based on the employment of the electrospinning technology.

3.1.1.3. Porosity

Notably, the resulting pristine *EN-PCLS* composed of microbeads and nanofibres displayed a fabric not only characterised by large surface area but also by excellent porosity of 86.6±2.6%. The nanoframeworks also displayed a wide range of pore size (from ultramicropores to mesopores similarly to what observed in soil) and a vast pore interconnectivity (Figs. 3c,e,f,g), which made it suitable to hosting microbes as in natural soils.[74]

3.1.1.4. Contact angle

PCL is a hydrophobic polymer.[90] The measurement of WCA of the deposited *EN-PCLS* showed that *EN-PCLS$_1$* was more hydrophobic (superhydrophobic) than the typical pristine electrospun PCL fabrics reported in the literature (156.34° vs 115–140°) (Fig. 4d). Differently, *EN-PCLS$_2$* appeared more hydrophilic (124.12°) than the other thicker mats deposited (Fig. 4d), as a consequence of the differences in the surface morphologies previously described. Such CA different values were maybe due to the formation of a Cassie−Baxter state in *EN-PCLS$_1$*, as the water drop did not penetrate the hollows of the grooved surface but remained suspended on top of the asperities forming a composite (solid-liquid-air) interface, as shown in Fig. 4d. Therefore, the water droplet reached an apparent 'equilibrium' contact angle to minimise the overall free energy of the system (as it does usually on flat surfaces) according to a Cassie–Baxter relationship, because of the nanoscale roughness.[91]

3.2. Bacteria biofilm development on the electrospun nanofabrics

In the comparison between the two *EN-PCLS*, *EN-PCLS$_1$* resulted too fragile so that the tall pinnacles and flakes easily degraded because of the mechanical friction with the liquid media occurring both under the stirring incubation required to obtain more durable and more specific bindings of bacteria to the nanostructures, and the following washings necessary to remove the unspecific interactions. Therefore, *EN-PCLS$_1$* resulted not suitable enough for the development of biofilms on the nanofabrics with repeatable results. On the other hand, the thick *EN-PCLS$_1$* framework was desirable because of a much larger surface exposed to interactions with microbes, a consequent higher adhesion and loading of larger quantities of bacteria per planar surface unit and then higher potential effectiveness and efficacy in the applications of interest. Hence, this framework requires to be further improved. As a consequence, the following steps of biofilm development here reported were focused on the interactions and behaviours of *B. terricola* cells with *EN-PCLS$_2$* only. If not specified, then, the electrospun nanostructured PCL scaffolds interacting with bacteria will be reported from now on as *EN-PCLS*.

3.2.1. Adhesion of bacteria cells to EN-PCLS

The bacterial colonisation of surfaces (biotic and abiotic) and biofilm development result from a series of events and processes inducing modifications in both bacteria cells and the surfaces.[92,93] The possibility for bacteria cells to interact with surfaces, colonise them and then possibly form biofilms requires at first that proximity between these two entities occurs. Usually, bacteria move towards target surfaces over a long-range scale driven by bacterial motility, in the case of bacterial species provided by specific appendages like flagella,[94] and physical forces, such as hydrodynamic forces, gravitational forces, Brownian motion, chemotactic or haptotactic attraction and additionally, over a short-range scale, i.e. when in proximity to the surfaces, by van der Waals and Coulomb forces and hydrophobic interactions.[95,96] In the experimental conditions here set up, the major long-range forces consisted of hydrodynamic forces consequent to the superimposed stirring of the incubation mixtures. The next step in the colonisation of abiotic or biotic surfaces by bacteria is the adhesion of cells to these surfaces. An extensive literature is available on the various degrees of interaction between bacteria and surfaces following distinct

phases.[92,97] However, although there are some studies concerning the development of electrospun coatings and scaffolds for suitable applications such as energy production and storage and pollutant removal,[15,21,22,98] the literature on interactions occurring between bacteria and nanofibres is still rare.[23,99–103] More recently, a more systematic study documented the early-stage interactions occurring between *B. terricola* cells and PCL nanofibres until microcolony formation.[24] In the present study, the investigation by SEM of the surfaces of *EN-PCLS* after 3 h incubation with B. terricola cells showed that additionally to the expected presence of bacteria, both microbeads and nanofibres after 3 h incubation appeared covered with an about 15 nm thick amorphous material (Figs. 3g and 6b for comparison) that consequently increased their dimensions relative to the pristine materials. It has been previously reported that PCL nanofibrous mats exposed to the incubation medium with *B. terricola* cells displayed similar morphological modifications.[24] This deposited material appeared as mostly located in the nanofibrous cavities of the honeycomb structures previously described (Fig. 5b, light blue arrows), while the aggregates of microbeads seemed to protrude from this coating (Fig. 5b, yellow arrows). At higher magnification, these materials deposited looked as forming thin membranes onto the nanofibrous network and in between the nanofibres (Figs. 5a and 6a, light blue arrows). The microbeads also seemed to be covered with such materials (Figs. 5, orange arrows, and 6c, yellow arrows), and the nanofibres appeared substantially larger than those typical of the pristine PCL nanofibres because of this coating (Figs. 3g; 4b; 6b, orange arrows). Such observations confirmed what already reported in a recent article describing the interactions of bacteria with nanofibres, where similar amorphous material coating electrospun nanofibrous frameworks incubated with the same bacteria species was classified as a conditioning film.[24] Conditioning films have been widely reported to be composed of organic compounds deriving from the media or produced by bacteria to make simpler the adhesion of bacterial cells to surfaces.[30,104] The composition of these materials depends on the bacteria species and growth and environmental (seasonal) conditions[30] and can include organic compounds displaying hydrophobic or hydrophilic properties, or both, such as proteins, polysaccharides, lipids, nucleic acids, humic acids, aromatic and amino acids.[105,106] In *Burkholderia cepacia*, polysaccharides were observed to be prevalent in EPS, relative to proteins.[30] In addition to the conditioning film, several little spheres of various size appeared widely spread on the nanofibres as well as grouped in clusters (Fig. 6a, yellow circles), or adhering to bacterial cells and at the interfaces between bacteria and nanofibres (Fig. 6b, pink arrows). These spheres have been identified as outer membrane vesicles (OMVs) and related to the formation of the conditioning film.[24]

After 3 h incubation only very few bacterial cells appeared adhering to the *EN-PCLS* (data not shown), while after 5 h incubation more bacteria were observed adhering to the nanostructured fabrics (Fig. 6a). Interestingly, bacteria were localised prevalently in the cavities of the honeycomb frameworks than in the walls of these structures or on single microbeads entrapped in the nanofibrous network (Fig. 6b, yellow and pink arrows, respectively). Interestingly, the cavities appeared to be the first areas of adhesion and dwelling of bacteria (Fig. 6a, orange arrows). Hence, the fabric structure seemed to have a remarkable role in facilitating the interaction of bacteria cells with these mats. The honeycomb wax cell-like cavities of the *EN-PCLS* maybe resulted in being sites more protected from stirring and where nutrients presumably tended to accumulate.

Moreover, it is worth noting that the cavities of *EN-PCLS*$_2$ appeared to be mostly composed of nanofibres and within these zones bacteria cells appeared adhering preferentially to nanofibres (Fig. 6a, orange arrows). On the contrary, Kargar et al. (2012) suggested that the interaction of bacteria with nanofibres, if ever, was due to the interplay with the material surface underneath the fibres and not specifically with them.[99] However, we observed that *B. terricola* cells often looked nicely as hanging on the nanofibres, then suggesting the occurrence of highly specific interactions between bacteria and these fibrous nanostructures (Fig. 6c, pink arrows). Such pieces of evidence were further confirmed by the very close interaction existing between bacteria cells and the nanofibres, despite the very different size between these two components (75.1 nm

of the average diameter of nanofibres - Fig. 4b - vs 500 nm of the average diameter of *B. terricola* cells) (Figs. 6b, green arrow, and 6c, red arrows). Similar results were reported in recent publications where the dependence of adhesion of the same bacteria cells on the size of PCL nanofibres was analysed, and bacteria were observed to adhere mostly to averaged 100 nm diameter nanofibres.[24] Likewise, when *Acinetobacter calcoaceticus* STB1 strain cells were found to have the highest bacterial immobilisation on polysulfone (PSU) fibres with random orientation and thinner diameter.[23]

Besides, bacteria appeared lying onto the nanofibres along their longitudinal axis, and also after duplication, they kept aligned along the same nanofibre, like in a rosary bead style (Figs. 6a and 6b, both with green arrows). Such alignment was maybe reinforced by the very close interaction between nanofibres and *B. terricola* cells, which led to the coalescence between the amorphous material surrounding *B. terricola* cells (maybe ascribable to the bacterial capsule, as in other species of the genus *Burkholderia*)[107] and the CF coating the nanofibres, as reported elsewhere[24] (Fig. 6b, pink arrows). On the contrary, a very few publications reported that bacteria cells never oriented longitudinally with the fibre axes when the latter have diameters smaller than those of bacteria, also generating distortion in the bacterial cell shapes and the general reduction of the bacterial adhesion.[99,100]

It is worth noting that, bacteria cells were almost absent on the aggregated microbeads composing the walls of the honeycomb structure of *EN-PCLS*$_2$ or on single microbeads entrapped in the nanofibrous network in the preliminary stages of colonisation (5 h incubation) (Fig. 6b, yellow and pink arrows, respectively). As evident, in the only cases when bacteria interacted with microbeads, the presence of nanofibres deposited on their surface looked to be required (Fig. 6c, red arrows). Interestingly, even after 48 h incubation, bacteria adhesion further extended to beads provided the latter were coated with nanofibres (Fig. 6d, light blue arrows); otherwise, the spheres appeared free of bacteria (Fig. 6d, orange arrows).

3.2.2. Anchoring of bacteria cells to EN-PCLS

After 28 h incubation, additional types of interactions between bacterial cells and the *EN-PCLS* were observed. *B. terricola* cells started forming appendages protruding throughout their surfaces following a radial distribution (Fig. 7a, orange arrows) to strengthen the anchoring to nanofibres and link also the cells each other (Fig. 7a, light blue arrows). The presence of appendages have been reported in other strains of *Burkholderia* genus and have been classified as fimbriae or pili.[108] Several publications considered these two terms interchangeable and used them indifferently to identify appendages.[109] Some distinctions, however, have been reported to distinguish different functions for these appendages such as adhesion, motility, DNA uptake and transfer, and formation of microcolonies.[110,111] Specifically, type 4 pili (T4P) have been demonstrated in *Burkholderia* to act as adhesins and then contribute to adhesion,[108,112] to be involved in twitching motility,[113] and to be the way DNA is absorbed from the outer environment and transferred from one cell to another starting from the type 4 secretion system (T4SS).[114] Additional to T4P, also cable pili have been described to play a role in adhesion in *Burkholderia*.[115] However, the precise identification of these appendages seems to be possible only upon the demonstration of particular genes or by using specific antibodies.[116,117] Hence, the analyses of the only aspects by SEM or TEM seem not to be capable of discriminating for sure between the distinct appendages.

The role of fimbriae in adhesion to surfaces has been associated with the presence of such appendages all around the bacteria cells (peritrichous pili).[118] Pili were also observed in the present study with a similar distribution (Fig. 7a, orange arrows), where they contributed to stabilising the linking of bacterial cells to the nanostructured fabrics against the shear strength due to stirring during the incubation. Comparable fimbriae have also been documented during the incubation of *B. terricola* cells with the nanofibrous-only PCL scaffolds.[24] Similar appendages were also observed in TEM micrographs of *EN-PCLS* incubated with bacteria (Fig. 7b green arrows), where the *B. terricola* cells attached to a microbead (here visible as a partial

cross-section delimited by a thick grey line (highlighted by an artificial violet line) (Fig. 7b). Such evidence might sound contrasting with the previous statement that bacteria cells never seemed to adhere to microbeads (§3.2.1). In the TEM micrograph, the microbead surface appeared further thickened, except a few areas (marked by pink arrows in Fig. 7b), by the presence of deposited CF, vesicles and/or solid spheres (Fig. 7b light blue, red and blue arrows). The bacteria cell in the figure, specifically, did not seem to anchor its fimbriae/pili directly to the microbead surface but to the rounded components laying on the CF coating the surface and acting as links between the appendages and the microbead surfaces (Fig. 7b, blue and red arrows). In detail, two types of rounded components seemed to be distinguished on the microbead surfaces, one showing a bright interior and another displaying an electron-dense core (Fig. 7b, blue and red arrows, respectively; inset: dotted blue and red rings, respectively). Some spherical components in the interface between bacteria cells and nanofibres were also documented in SEM micrographs (Fig. 6b, pink arrows). Rounded elements with an electron-dense core were also reported in other papers at the interface between bacteria cells and nanofibres, where they were identified as outer membrane vesicles (OMVs) and were suggested to be involved in linking these two entities.[24] (OMVs are nano-sized spheroid particles generated in several Gram-negative bacteria from the protuberances of the outer membrane.[119,120] Differently, the bright core rounded components were here identified as the cross-section of nanofibres and confirmed the presence of laying nanofibres onto the sphere where bacteria are linked, as observed in several other pictures (Figs. 6c,d). Analogous spherical structures also were observed in other TEM micrographs (Fig. 7d, orange arrows). The TEM images of longitudinal and transversal sections of electrospun PCL nanofibres linked to bacterial cells observed in other studies seemed to support the identification of the bright core rounded components linked to bacteria here captured by TEM with nanofibre cross-sections.[24] Hence, the hypothesis that *B. terricola* cells appeared to adhere preferentially to PCL nanofibres and were linked to microbead surfaces only in the sites where nanofibres were deposited and acted as mediators (§3.2.1) seemed to be confirmed. Additional to the fimbriae joining bacteria to the nanofibrous network, similar appendages were also observed linking adjacent bacterial cells (Fig. 7a, light blue arrows). Various types of pili have been described connecting bacteria[121] and have been related to the DNA transfer and exchange between them (F-type, P-type or I-type pili).[122] Appendages with a similar aspect have also been described recently in *B. terricola* cells grown on PCL nanofibres.[24]

3.2.3. Colonisation of EN-PCLS and biofilm formation

B. terricola cells started forming microcolonies few hours after the adhesion of bacteria to the nanofibres of the *EN-PCLS* (§3.2.1), so that some of them, despite very few, could already be observed at 5 h incubation in the honeycomb structure, where rod-like bacteria begun to replicate while hanging on the nanofibres, thus forming bizarre suspended microcolonies composed of about 50 cells (Fig. 8a).

By increasing the incubation and the contact with the *EN-PCLS* (20 h), the microcolonies enlarged but always growing preferentially over the nanofibres and the nanofibrous frameworks, thus generating masses of bacteria appearing hanging on nets of tiny nanofibres (Fig. 8b). While the adhesion of bacteria started becoming more stable because of appendages-mediated interactions (28 h) (§3.2.2), the further extensive replication drove the bacterial population to a vast colonisation of the fabrics, also accompanied by new adhesions of cells to the nanofibres of the *EN-PCLS*, globally forming a monolayer (Fig. 8c). Interestingly, *B. terricola* cells at this stage of growth and on started showing modifications in the morphology since in SEM micrographs they appeared to lose the 1.5 µm long rod-like shape (Figs. 5c, 6a,b,c) in favour of egg-shaped (Figs. 7a and 7c, not indicated with green arrows) and until more spherical forms (Fig. 6d, and 7a and 7c, both with green arrows). Such findings might be explained by the nutrient availability rather than the growth rate as the major factor of size determination so that under nutrient-poor conditions, cell size is reduced.[123] Alternatively, such morphological

alterations stimulated in the bacteria by the prolonged interactions with the *EN-PCLS* might be part of the phenotypical trait modifications mediated by gene expression upon sensing the specific nanofibrous morphology of the surface and inducing the switch from the planktonic to the stable sessile form.[31,124]

Additionally, bacteria at early stages of incubation and interactions (5-28 h incubation) with nanofibres displayed several OMVs protruding and bound at the cell surface, when observed by SEM (Fig. 6b, pink arrows). By increasing the period of incubation, bacteria prevalently appeared in SEM micrographs with less or free of OMVs at the surface (Fig. 7a,c). Such evidence seemed to support the hypothesis further that OMVs, in the present study, were involved in the early stages of bacterial adhesion to surfaces (nanofibrous fabrics).[24,125] OMVs have been frequently reported in the literature to be related to biofilm formation[126] because the content of these structures has been proven to take part of the matrix composition of biofilms.[127] Indications about changes in the presence of OMVs on bacteria during the incubation confirmed the different phenotypical traits of *B. terricola* cells occurring during the transition from adhesion towards biofilm development.

During this stage of colonisation, bacteria spread throughout the nanofibrous network within the honeycomb wax cell-like structures (28 h) (Fig. 7a,c, 8c), while dissimilarly, microbes dwelling the PCL microbeads composing the honeycomb wax cell-like walls displayed a different behaviour in the colonisation. In these areas, bacteria formed large microcolonies prevalently occupying the spaces in between the microbeads (Fig. 8d). Notably, the colonisation of the spaces between the microbeads always occurred in the presence of the nanofibrous network, which enabled the microbial adhesion, as well as colony formation and growth (Fig. 8c, pale blue arrows). A similar occurrence was observed when a further increase in the bacterial population generated more massive colonies (macrocolonies) (48 h) (Fig. 9a, pale blue arrows). Interestingly, in both 3D micro- and macrocolonies, holes crossing and in between the colonies were visible (Fig. 8a,b,d and 9a, orange arrows). In *Pseudomonas aeruginosa*, it has been proven that such feature is linked to the synthesis of surfactants aimed at keeping open channels surrounding macrocolonies,[128] maybe to permit the inflow and outflow of water, nutrients and wastes.

The organisation of bacteria in colonies and 3D structured biofilms have been related to several factors. In P. aeruginosa, a biofilm development model has been suggested to explain the influence of nutrients on the structure of bacteria biofilms. Specifically, when using glucose as substrate, some subpopulations tend to form cell aggregates (stalk) of micro- and macrocolonies, alternated with carpets of cells in flat layers, and globally resulting in 3D structured biofilms, while the growth on glutamate and citrate stimulate only the formation of flat, uniform biofilms.[129,130] In the present study, *B. terricola* cells were grown on glucose as C source and presented both flat and 3D structured growth, as aforementioned (Fig. 8 and 9a). Furthermore, the formation of microcolonies and mostly macrocolonies has also been reported to follow the synthesis and release out of the cells of extracellular polymeric substances (EPS) and other matrix components.[131,132] EPS are the major component of the matrix of biofilms, consisting of a collection of different types of biopolymers mainly composed of neutral, charged and hydrophobic polysaccharides, proteins (both enzymatic and non-enzymatic), extracellular DNA (eDNA), humic substances, biosurfactants and lipids.[133,134] The synthesis and release of EPS are under the expression of genes that are often activated by bacterial molecular signals related to the population density when a threshold concentration of these signals is achieved in a specific site (quorum sensing).[131] Both the cited effects of nutrients and EPS on colony formation have been related to the cell motility reduction and the selection of immobile subpopulations of bacteria inducing the development of 3D cell aggregations like micro- and macrocolonies up to the formation of biofilms, sometimes displaying mushroom architectures.[130]

Moreover, it has been reported that the secretion of EPS is higher when motility is reduced.[130] EPS have also been demonstrated to be involved in both the adhesion and the following stable attachment and immobilisation of cells consequent to the embedment of bacteria in the same

matrix, then also facilitating both cell-cell recognition and the expansion of bacterial populations and the formation of micro- and macrocolonies.[133–135] Hence, EPS constitute a significant factor contributing to the development of biofilms onto surfaces.[92] They also play additional remarkable functions such as facilitating the interactions between bacteria and surfaces to nutrients and water sorption and retention, nutrient storage and cycling (by enzyme activities), protection from adverse agents and stresses, and genetic exchange.[133–135]

In the present study, the contribution of EPS in the formation of stable interactions of bacteria with the *EN-PCLS* was observed over time (i.e. from 5 h to 48 h incubation), with bacteria cells progressively enveloped and eventually embedded by EPS at later stages of the exponential growth on the nanostructured fabrics (28-48 h), i.e. when colonies were formed (Figs. 7a,c, 8a,b but mostly in Fig. 9b). TEM micrographs confirmed the presence of EPS surrounding the bacteria at these stages, where such materials appeared as dark halos around the cells (Figs. 9c). The assessment of the vital and metabolically active *B. terricola* cells by INT during the biofilm development on the nanostructured fabrics supported the presence of various phases of bacterial growth observed in SEM micrographs. As shown in Fig. 10, the evolution of the *B. terricola* cells interaction with *EN-PCLS* from the first phases of adhesion (5 h) (10a) until a more stable attachment and colonisation (48 h) (10b) were characterised by a striking increase in the red colour of the colonised the nanostructured fabrics due to the remarkable reduction of INT to its formazan consequent to the presence of a larger and diffused bacterial population. Based on the presence of the red colour, it is evident that the colonisation of the *EN-PCLS* occurred at first at the borders of the mats and then proceeded inwards (Fig. 10a) and spread throughout the nanoframework (Fig. 10b). Moreover, based on the quantification of INT reduction over time, the high rate of cell division induced by the incubation conditions led to an exponential growth of the *B. terricola* population adhering to the mat, where cell numbers increased logarithmically until 48 h incubation with an extensive colonisation of the *EN-PCLS* (Fig. 10c) accompanied by the formation of several micro- and macrocolonies formerly observed in the SEM micrographs (Figs. 6,7,8,9). Afterwards, this intensive growth decreased, maybe since the limitation of nutrients in the incubation (spent) medium caused stress in bacteria and/or the accumulation of toxic metabolic products. It is reported that nutrient limitation favours biofilm development,[136,137] probably because its formation enables bacteria to resist adverse conditions like nutrient deficiency.[6] As a consequence, the bacterial population entered in the stationary phase, i.e. where cell division was balanced by cell death that started to happen (7 d incubation) (Fig. 10c). Notwithstanding, from 48 h to 7 d incubation, the additional extensive release of EPS by *B. terricola* cells contributed to creating a hydrated biopolymer network comprising the biofilm matrix that seemed to support the response of bacteria cells to unfavourable nutritive conditions. EPS have been reported acting as a nutrient reservoir concentrating substances based on the combination of sorptive and degrading properties, for the presence of extracellular enzymes.[135] The released EPS, surrounding at first single bacterial cells, contributed to fuse them with adjacent cells, thus further enhancing cell-cell communication until generating a composite layer of densely packed bacteria embedded in these organic materials and globally forming a uniform coating covering the *EN-PCLS*, thus demonstrating the development of a proper despite young biofilm (*BEN-PCLS*) (Fig. 11a). The overview of the *BEN-PCLS* showed that, because of the extensive presence of the EPS coating, the original honeycomb wax cell-like architecture of the nanostructured fabrics was hardly identifiable, at this microbial growth level (Fig. 11b, dotted yellow circles).

It is worth noting that, despite such an extensive colonisation and the large bacterial population developed in the *EN-PCLS* until 7 d incubation, microbeads deprived of nanofibres deposited on them still appeared free of any bacteria adhering on their surfaces (Fig. 11a, green arrows). On the contrary, the microbeads with nanofibres laying on their surfaces housed bacteria cells so that the larger the number of deposited nanofibres on them, the higher the number of bacteria attached to them (Fig. 11a, pale blue arrows). Hence, it is further confirmed that at least in the case of PCL scaffolds interacting with *B. terricola* cells, the preferential adhesion of these

bacteria occurred onto nanofibres, although flat-like surfaces were present. Such finding further supports the hypothesis that the condition enabling and guaranteeing or at least favouring bacterial adhesion to surfaces is the presence of nanofibres with diameters smaller than that of bacteria cells.

In real soils, it is very difficult to find conditions of early colonisation of soil particles by microbes. Microorganisms usually occupy only a small fraction of the soil volume (0.001%), in spite of their large number (10^8-10^{10} g^{-1} soil), so that they are mostly present in hotspots or in "patch-like" distributions, where substrates, nutrients and favourable environmental conditions are present.[138,139] Moreover, organic materials released from organic structures degradation by microbial populations are constantly present in the soil solution as dissolved organic carbon (DOC) and water soluble organic matter (WSOM)[140,141] and frequently tend to deposit onto particle surfaces as a conditioning film.[142] Hence, in the colonised sites, huge amounts of EPS are deposited onto particles and diffused biofilms coat the surfaces, thus hindering a clear detection of possible fibrous materials underneath.[143]

The further evolution of the biofilm showed several areas in the nanostructured scaffolds where the massive production and release of EPS was quantitatively so remarkable to form a fairly thick matrix embedding both the bacteria cells and the nanofibrous frameworks and appearing as a continuous coating like a blanket (Figs. 11c, pink arrowheads) typical of a mature biofilm (*BEN-PCLS*). In such 3D architecture, bacterial colonies were hardly visible from the matrix except for some spots appearing like rocks protruding from the sea (Figs. 11b, green arrowheads). Interestingly, in the biofilm structure, some holes were observed suitable to enable water, nutrients, oxygen, and wastes flowing through the *BEN-PCLS*, and thus permitting bacterial feeding and toxic metabolic byproducts removal (Figs. 11b,c, yellow arrowheads). Hence, within 7 d incubation, *B. terricola* cells were successful in growing and developing a mature 3D biofilm onto the nanostructured PCL framework here created and aimed at mimicking the soil architecture.

3.2.4. Degradation of Biofilmed EN-PCLS (BEN-PCLS)

The extended incubation of *BEN-PCLS* until 11 d highlighted that bacteria after 7 d were still in the stationary phase, and this condition persisted until the end of the incubation here tested, based on INT measurements (Figure 10c). Nevertheless, notwithstanding the growth conditions appeared still supporting a constant bacterial population, SEM micrographs showed that a partial degradation of the *B. terricola* biofilm architecture occurred (Fig. 12). In detail, the coating previously observed covering the whole *BEN-PCLS* appeared extensively ripped in numerous zones (Fig. 12a, green arrows), thus exposing the nanoframeworks underneath and the colonising bacteria (Fig. 12b). The various nanostructures of the scaffolds (nanofibres and microbeads) also appeared fragmented and degraded (Fig. 12b, orange and pink arrows, respectively). Interestingly, consequent to such disintegration, the EPS coating covering the underlying colonised nanofabrics observed in Fig. 11 and participating the biofilm architecture displayed a multilayered organisation (for the first time to our knowledge) in SEM micrographs with large magnification (14,000 X) (Fig. 12d, yellow arrows), which in some cases achieved 10-20 µm thickness (Fig. 12d, pale blue arrows). The presence of a stationary phase lasting at least from 7 d to 11 d, based on no substantial decrease in the *B. terricola* population typical of a transition to the death phase (Fig. 10c), might reasonably induce to speculate that the presumable limitation of C sources in the medium (causing the decrease in microbial population from 48 h to 7 d) was instead sufficiently compensated, at this stage of incubation, by the decomposition of the organic structure of *EN-PCLS* by bacteria cells.

Hence, in the present study, the various SEM micrographs of *EN-PCLS* collected at distinct periods of incubation with *B. terricola* cells provided insights on how bacteria interacted with the beads-&-fibres material here created and mimicking the typical spatial architecture of soils composed of mineral particles and organic matter, respectively (Fig. 13). Noteworthy, it was also displayed how bacteria spatially organised their community in 3D biofilms when the substrate

for biofilm development was three-dimensional as in most of the natural contexts, and not as simple as in most of the contexts studied in the literature. In addition, the EPS released by *B. terricola* during the incubation not only formed a matrix embedding bacteria cells in layers at micro-sized scale, but also enclosed both nanofibres and microspheres on a large scale and finally formed a thick layer that like a blanket coated the whole 3D framework resembling what observed in soil (Fig. 13). Therefore, the 3D nanostructured scaffold here fabricated provided substantial benefits to the development of a stable residential bacterial population, since the honeycomb-like spatial configuration facilitated the accumulation of nutrients and the interception of planktonic bacteria, and created comfortable sites for bacterial adhesion. Furthermore, the nanoframework showed a broad, porous distribution including micropores and mesopores typically suitable to harbouring microbial cells, which also favoured their anchorage and the EPS release that induced microbial proliferation in micro- and macrocolonies until the mature biofilm generation and the formation of a thick coating over the whole fabric. As a consequence, the bacterial population housed in such 3D nanostructured scaffold resulted highly protected from external adverse conditions.

4. CONCLUSIONS

The novelty of the present study laid in the creation of a 3D self-standing, porous, and nanostructured scaffold. Such features made it very different from the smooth and flat surfaces of the metal, silicon and plastic materials typically used in industrial plant infrastructures, medical implants and devices and energy generation and storage systems that have been traditionally studied in interactions with bacteria. Even when 3D nanofibrous structures were investigated, in very few cases,[15] only fibres typically comprised those mats, instead of the beads-&-fibres framework here proposed. Moreover, the fibres included in the present 3D nanoscaffold were much thinner in diameter, and the overall fabric was taller than those utilised in the other studies.[15] The model artificial nanostructured framework here proposed provided the evidence that the *B. terricola* bacterial cells appeared capable of discriminating between nanofibrous and nanofibre-free flat surfaces of microbeads and preferring the former for adhesion. The relationship between microbeads, nanofibres and bacteria, and the growth of the microbes until biofilm formation, then, was also original.

Furthermore, the present study demonstrated that:

- Electrospinning technology was capable of creating porous nanostructured frameworks composed of fibres and beads intending simulating the soil architecture (Fig. 13).
- Such soil-like nanoscaffolds were capable of providing *B. terricola* cells a suitable environment to adhere, exponentially grow as it happens in planktonic cultures and liquid media, and develop mature biofilms (Fig. 13).
- At the same time, *B. terricola* cells were capable of colonising such *EN-PCLS* without suffering for the adhesion to the nanostructured scaffolds.
- The bacteria populations growing in the incubation conditions here applied and on the porous nanostructured supports here created were capable of retaining their vitality until the formation of the biofilm although with a predictable reduction in the total population and the relative metabolic activity consequent to the limitation of nutrients.
- The nanostructured scaffolds here created provided an exceptional opportunity to visualise and study the step-by-step development of bacterial biofilms on 3D soil-like architectures and most of all to observe the overall organisation of bacterial biofilms formed in such conditions, thus providing more reliable information on how biofilms are organised in real soils (Fig. 13).

The remarkable achievements of the nanostructured soil-like architecture here proposed enable a series of potential improvements in various fields through the possible development of nanobiotechnological carrier materials for applications as both functional coatings of surfaces and functional self-standing tools to be spread in specific applications (biofilmed membrane coatings and biofilmed scaffolds as carriers, respectively):

- Development of self-standing nanobiotechnological carriers for applications in agriculture such as:
  - more effective biostimulants acting as biofertilisers, biopesticides or both
  - more effective amendments to improve soil structure.
- Development of self-standing nanotools and coatings as nanobiotechnological carriers for applications in the environment like:
  - filters, membranes and pellets for the removal of pollutants from wastewater and soil
  - coatings for containers for the removal of pollutants from wastewater, and cleaning drinking water and other liquids.
- Development of self-standing nanotools and coatings as nanobiotechnological carriers for industrial applications like:
  - biofilm-housing scaffolds for spreading bacteria in liquid media in bioreactors where playing processes of interest (e.g. compound degradation, biomolecule synthesis and transformation)
  - coatings for containers and pipes and drains suitable for processing substances in flowing liquid media.

5. CONFLICTS OF INTEREST

There are no conflicts to declare.

6. ACKNOWLEDGMENT

The authors gratefully acknowledge Dr. A.R. Taddei for sample preparations for Scanning Electron Microscopy (SEM) and Transmission Electron Microscopy (TEM) and investigations at the Electron Microscopy Section of the High Equipment Centre, at Tuscia University (Viterbo, Italy). The authors further thank the COST Action MP1206 “Electrospun nano-fibres for bioinspired composite materials and innovative industrial applications” that promoted the present activity and the collaboration between scientists.

7. REFERENCES

1 K. C. Marshall, *Planktonic Versus Sessile Life of Prokaryotes*, in *The Prokaryotes*, eds. E. Rosenberg, E. F. DeLong, S. Lory, E. Stackebrandt and F. Thompson, Springer, Berlin, Heidelberg, 2013, pp. 191–201.

2 J. Kreth and M. C. Herzberg, *Molecular Principles of Adhesion and Biofilm Formation*, in *The Root Canal Biofilm*, eds. L. E. Chávez de Paz, C. M. Sedgley and A. Kishen, Springer-Verlag, Berlin Heidelberg, 2015, pp. 23–53.

3 H.-C. Flemming, J. Wingender, U. Szewzyk, P. Steinberg, S. A. Rice and S. Kjelleberg, Biofilms: an emergent form of bacterial life, *Nat. Rev. Microbiol.*, 2016, **14**, 563–575.

4 C. Matz, *Biofilms as Refuge against Predation*, in *The biofilm mode of life: mechanisms and adaptations*, eds. S. Kjelleberg and M. Givskov, Horizon Bioscience, Norfolk, UK, 2007, pp. 195–213.

5 E. van Duijkeren, A.-K. Schink, M. C. Roberts, Y. Wang and S. Schwarz, Mechanisms of Bacterial Resistance to Antimicrobial Agents, *Microbiol. Spectr.*, 2018, **6**, 51–82.

6 O. Rendueles and J.-M. Ghigo, Mechanisms of Competition in Biofilm Communities, *Microbiol Spectr.*, 2015, **3**, MB-0009-2014.

7 N. Nocelli, P. Bogino, E. Banchio, W. Giordano, N. Nocelli, P. C. Bogino, E. Banchio and W. Giordano, Roles of Extracellular Polysaccharides and Biofilm Formation in Heavy Metal Resistance of Rhizobia, *Materials (Basel).*, 2016, **9**, 418.

8 X. Sheng, Y. P. Ting and S. O. Pehkonen, The influence of ionic strength, nutrients and pH on bacterial adhesion to metals, *J. Colloid Interface Sci.*, 2008, **321**, 256–264.

9 C. R. Kokare, S. Chakraborty, A. N. Khopade and K. R. Mahadik, Biofilm: Importance and applications, *Indian J. Biotechnol.*, 2009, **8**, 159–168.

10 H. H. Tuson and D. B. Weibel, Bacteria-surface interactions, *Soft Matter*, 2013, **9**, 4368–4380.

11 T. Rudrappa, M. L. Biedrzycki and H. P. Bais, Causes and consequences of plant-associated biofilms, *FEMS Microbiol. Ecol.*, 2008, **64**, 153–166.

12 M. Rafique, K. Hayat, T. Mukhtar, A. A. Khan, M. S. Afridi, T. Hussain and T. Sultan, *Bacterial Biofilm Formation and Its Role against Agricultural Pathogens*, in *The Battle Against Microbial Pathogens: Basic Science, Technological Advances and Educational Programs*, ed. A. Méndez-Vilas, Formatex, Badajoz, 2015, pp. 373–382.

13 M. E. Galelli, G. C. Sarti and S. S. Miyazaki, Lactuca sativa biofertilization using biofilm from Bacillus with PGPR activity, *J. Appl. Hortic.*, 2015, **17**, 186–191.

14 D. Ercan and A. Demirci, Current and future trends for biofilm reactors for fermentation processes, *Crit. Rev. Biotechnol.*, 2015, **35**, 1–14.

15 S. Chen, H. Hou, F. Harnisch, S. A. Patil, A. A. Carmona-Martinez, S. Agarwal, Y. Zhang, S. Sinha-Ray, A. L. Yarin, A. Greiner and U. Schröder, Electrospun and solution blown three-dimensional carbon fiber nonwovens for application as electrodes in microbial fuel cells, *Energy Environ. Sci.*, 2011, **4**, 1417–1421.

16 N. A. Anjum, *Chemical Pollution Control with Microorganisms*, Nova Science Publishers Inc, 2017.

17 M. Das and A. Adholeya, *Role of Microorganisms in Remediation of Contaminated Soil*, in *Microorganisms in Environmental Management: Microbes and Environment*, eds. T. Satyanarayana, B. N. Johri and A. Prakash, Springer Netherlands, Dordrecht, 2012, pp. 81–111.

18 M. Asri, S. Elabed, S. Ibnsouda Koraichi and N. El Ghachtouli, *Biofilm-Based Systems for Industrial Wastewater Treatment*, in *Handbook of Environmental Materials Management*, ed. C. M. Hussain, Springer, Cham, 2018, pp. 1–21.

19 H. Leonard, S. Halachmi, N. Ben-Dov, O. Nativ and E. Segal, Unraveling antimicrobial susceptibility of bacterial networks on micropillar architectures using intrinsic phase-shift spectroscopy, *ACS Nano*, 2017, **11**, 6167–6177.

20 V. K. Truong, S. Rundell, R. Lapovok, Y. Estrin, J. Y. Wang, C. C. Berndt, D. G. Barnes, C. J. Fluke, R. J. Crawford and E. P. Ivanova, Effect of ultrafine-grained titanium surfaces on adhesion of bacteria, *Appl. Microbiol. Biotechnol.*, 2009, **83**, 925–937.

21 S. Cavaliere, *Electrospinning for Advanced Energy and Environmental Applications*, CRC Press, Boca Raton, 2015.

22 B. Balusamy, O. F. Sarioglu, A. Senthamizhan and T. Uyar, Rational Design and Development of Electrospun Nanofibrous Biohybrid Composites, *ACS Appl. Bio Mater.*, 2019, **2**, 3128–3143.

23 O. F. Sarioglu, A. Celebioglu, T. Tekinay and T. Uyar, Evaluation of fiber diameter and morphology differences for electrospun fibers on bacterial immobilization and bioremediation performance, *Int. Biodeterior. Biodegradation*, 2017, **120**, 66–70.

24 F. De Cesare, E. Di Mattia, E. Zussman and A. Macagnano, A Study on the Dependence of Bacteria Adhesion on the Polymer Nanofibre Diameter, *Environ. Sci. Nano*, 2019, **6**, 778–797.

25 S. L. Woo and O. Pepe, Microbial consortia: Promising probiotics as plant biostimulants for sustainable agriculture, *Front. Plant Sci.*, 2018, **9**, 1801.

26 D. Kour, K. L. Rana, A. N. Yadav, N. Yadav, M. Kumar, V. Kumar, P. Vyas, H. S. Dhaliwal and A. K. Saxena, Microbial biofertilizers: Bioresources and eco-friendly technologies for agricultural and environmental sustainability, *Biocatal. Agric. Biotechnol.*, 2020, **23**, 101487.

27 V. K. Singh, S. Das, A. K. Dwivedy, R. Rathore and N. K. Dubey, Assessment of chemically characterized nanoencapuslated Ocimum sanctum essential oil against aflatoxigenic fungi contaminating herbal raw materials and its novel mode of action as methyglyoxal inhibitor, *Postharvest Biol. Technol.*, 2019, **153**, 87–95.

28 S. Das, *Microbial Biodegradation and Bioremediation*, Elsevier, 2014.

29 L. M. Kaminsky, R. V. Trexler, R. J. Malik, K. L. Hockett and T. H. Bell, The Inherent Conflicts in Developing Soil Microbial Inoculants, *Trends Biotechnol.*, 2019, **37**, 140–151.

30 G. Hwang, S. Kang, M. G. El-Din and Y. Liu, Impact of an extracellular polymeric substance (EPS) precoating on the initial adhesion of Burkholderia cepacia and Pseudomonas aeruginosa, *Biofouling*, 2012, **28**, 525–538.

31 K. Otto and T. J. Silhavy, Surface sensing and adhesion of Escherichia coli controlled by the Cpx-signaling pathway, *Proc. Natl. Acad. Sci. U. S. A.*, 2002, **99**, 2287–2292.

32 C. M. Bhadra, M. Werner, V. A. Baulin, V. K. Truong, M. Al Kobaisi, S. H. Nguyen, A. Balcytis, S. Juodkazis, J. Y. Wang, D. E. Mainwaring, R. J. Crawford and E. P. Ivanova, Subtle Variations in Surface Properties of Black Silicon Surfaces Influence the Degree of Bactericidal Efficiency, *Nano-Micro Lett.*, 2018, **10**, 36.

33 A. J. T. Teo, A. Mishra, I. Park, Y. J. Kim, W. T. Park and Y. J. Yoon, Polymeric Biomaterials for Medical Implants and Devices, *ACS Biomater. Sci. Eng.*, 2016, **2**, 454–472.

34 B. Halan, K. Buehler and A. Schmid, Biofilms as living catalysts in continuous chemical syntheses, *Trends Biotechnol.*, 2012, **30**, 453–465.

35 A. L. Yarin, B. Pourdeyhimi and S. Ramakrishna, *Fundamentals and Applications of Micro and Nanofibers*, Cambridge University Press, 2014.

36 S. Haider, Y. Al-Zeghayer, F. A. Ahmed Ali, A. Haider, A. Mahmood, W. A. Al-Masry, M. Imran and M. O. Aijaz, Highly aligned narrow diameter chitosan electrospun nanofibers, *J. Polym. Res.*, 2013, **20**, 105.

37 B. Ding, M. Wang, X. Wang, J. Yu and G. Sun, Electrospun nanomaterials for ultrasensitive sensors, *Mater. Today*, 2010, **13**, 16–27.

38 A. Celebioglu and T. Uyar, Electrospun porous cellulose acetate fibers from volatile solvent mixture, *Mater. Lett.*, 2011, **65**, 2291–2294.

39 X. Hu, S. Liu, G. Zhou, Y. Huang, Z. Xie and X. Jing, Electrospinning of polymeric nanofibers for drug delivery applications, *J. Control. Release*, 2014, **185**, 12–21.

40 A. Macagnano, E. Zampetti and E. Kny, *Electrospinning for High Performance Sensors*, Springer, Cham, 2015.

41 T. Uyar and E. Kny, *Electrospun Materials for Tissue Engineering and Biomedical Applications : Research, Design and Commercialization*, Woodhead Publishing Ltd, 2017.

42 S. Torres-Giner, *Electrospun Nanofibers for Food Packaging Applications*, in *Multifunctional and Nanoreinforced Polymers for Food Packaging*, ed. J. M. Lagaron, Elsevier, Cambridge, 2011, pp. 108–125.

43 M. Mirjalili and S. Zohoori, Review for application of electrospinning and electrospun nanofibers technology in textile industry, *J. Nanostructure Chem.*, 2016, **6**, 207–213.

44 A. Smeets, C. Clasen and G. Van den Mooter, Electrospraying of polymer solutions: Study of formulation and process parameters, *Eur. J. Pharm. Biopharm.*, 2017, **119**, 114–124.

45 V. M. Entov and A. L. Yarin, Influence of elastic stresses on the capillary breakup of jets of dilute polymer solutions, *Fluid Dyn.*, 1984, **19**, 21–29.

46 A. Yarin, *Free Liquid Jets and Films: Hydrodynamics and Rheology*, Longman Pub Group, 1996.

47 W. Ning, P. Shang, J. Wu, X. Shi and S. Liu, Novel amphiphilic, biodegradable, biocompatible, thermo-responsive ABA triblock copolymers based on PCL and PEG analogues via a combination of ROP and RAFT: Synthesis, characterization, and sustained drug release from self-assembled micelles, *Polymers*, 2018, **10**, E214.

48 Z. Heydari, D. Mohebbi-Kalhori and M. S. Afarani, Engineered electrospun polycaprolactone (PCL)/octacalcium phosphate (OCP) scaffold for bone tissue engineering, *Mater. Sci. Eng. C*, 2017, **81**, 127–132.

49 L. Jiang, L. Wang, N. Wang, S. Gong, L. Wang, Q. Li, C. Shen and L. S. Turng, Fabrication of polycaprolactone electrospun fibers with different hierarchical structures mimicking collagen fibrils for tissue engineering scaffolds, *Appl. Surf. Sci.*, 2018, **427**, 311–325.

50 G. Zhou, H. Jiang, Z. Yin, Y. Liu, Q. Zhang, C. Zhang, B. Pan, J. Zhou, X. Zhou, H. Sun, D. Li, A. He, Z. Zhang, W. Zhang, W. Liu and Y. Cao, In Vitro Regeneration of Patient-specific Ear-shaped Cartilage and Its First Clinical Application for Auricular Reconstruction, *EBioMedicine*, 2018, **28**, 287–302.

51 E. Mahenthiralingam, T. A. Urban and J. B. Goldberg, The multifarious, multireplicon *Burkholderia cepacia* complex, *Nat. Rev. Microbiol.*, 2005, **3**, 144–156.

52 A. A. Angus, C. M. Agapakis, S. Fong, S. Yerrapragada, P. Estrada-de los Santos, P. Yang, N. Song, S. Kano, J. sus Caballero-Mellado, S. M. de Faria, F. D. Dakora, G. Weinstock and A. M. Hirsch, Plant-Associated Symbiotic *Burkholderia* Species Lack Hallmark Strategies Required in Mammalian Pathogenesis, *PLoS One*, 2014, **9**, e83779.

53 S. W. Ali, F. Yu, L. Li, X. Li, L. Gu, J. Jiang and S. Li, Studies revealing bioremediation potential of the strain *Burkholderia* sp. GB-01 for abamectin contaminated soils, *World J. Microbiol. Biotechnol.*, 2012, **28**, 39–45.

54 M. Muganu, M. Paolocci, C. Bignami and E. Di Mattia, Enhancement of adventitious root differentiation and growth of in vitro grapevine shoots inoculated with plant growth promoting rhizobacteria, *Vitis - J. Grapevine Res.*, 2015, **54**, 73–77.

55 G. C. Alves, A. V. de Matos Macedo, F. B. dos Reis, S. Urquiaga and V. M. Reis, Plant growth promotion by four species of the genus *Burkhoderia*, *Plant Soil*, 2016, **399**, 373–387.

56 W. Otten, R. Pajor, S. Schmidt, P. C. Baveye, R. Hague and R. E. Falconer, Combining X-ray CT and 3D printing technology to produce microcosms with replicable, complex pore geometries, *Soil Biol. Biochem.*, 2012, **51**, 53–55.

57 K. Cazelles, W. Otten, P. C. Baveye and R. E. Falconer, Soil fungal dynamics: Parameterisation and sensitivity analysis of modelled physiological processes, soil architecture and carbon distribution, *Ecol. Modell.*, 2013, **248**, 165– 173.

58 I. Y. Enis, J. Vojtech and T. G. Sadikoglu, Alternative solvent systems for polycaprolactone nanowebs via electrospinning, *J. Ind. Text.*, 2017, **47**, 57–70.

59 K. Kanjanapongkul, S. Wongsasulak and T. Yoovidhya, Investigation and Prevention of Clogging During Electrospinning of Zein Solution, *J. Appl. Polym. Sci.*, 2010, **118**, 1821–1829.

60 D. Nečas and P. Klapetek, Gwyddion: An open-source software for SPM data analysis, *Cent. Eur. J. Phys.*, 2012, **10**, 181–188.

61 A. F. Stalder, T. Melchior, M. Müller, D. Sage, T. Blu and M. Unser, Low-bond axisymmetric drop shape analysis for surface tension and contact angle measurements of sessile drops, *Colloids Surfaces A Physicochem. Eng. Asp.*, 2010, **364**, 72–81.

62 A. F. Stalder, G. Kulik, D. Sage, L. Barbieri and P. Hoffmann, A snake-based approach to accurate determination of both contact points and contact angles, *Colloids Surfaces A Physicochem. Eng. Asp.*, 2006, **286**, 92–103.

63 S. Soliman, S. Sant, J. W. Nichol, M. Khabiry, E. Traversa and A. Khademhosseini, Controlling the porosity of fibrous scaffolds by modulating the fiber diameter and packing density, *J. Biomed. Mater. Res. - Part A*, 2011, **96A**, 566–574.

64 R. A. Moore, A. Tuanyok and D. E. Woods, Survival of *Burkholderia pseudomallei* in water, *BMC Res. Notes*, 2008, **1**, 11.

65 S. Rodrigues, C. Paillard, G. Le Pennec, A. Dufour and A. Bazire, Vibrio tapetis, the causative agent of Brown Ring Disease, forms biofilms with spherical components, *Front. Microbiol.*, 2015, **6**, 1384.

66 J. C. Stockert, R. W. Horobin, L. L. Colombo and A. Blázquez-Castro, Tetrazolium salts and formazan products in Cell Biology: Viability assessment, fluorescence imaging, and labeling perspectives, *Acta Histochem.*, 2018, **120**, 159–167.

67 J. Villegas-Mendoza, R. Cajal-Medrano and H. Maske, INT (2-(4-Iodophenyl)-3-(4-Nitrophenyl)-5-(Phenyl) Tetrazolium Chloride) Is Toxic to Prokaryote Cells Precluding Its Use with Whole Cells as a Proxy for In Vivo Respiration, *Microb. Ecol.*, 2015, **70**, 1004–1011.

68 T. I. Ladd and J. W. Costerton, 9 Methods for Studying Biofilm Bacteria, *Methods Microbiol.*, 1990, **22**, 285–307.

69 X. Peng, R. Horn and P. Hallett, Soil structure and its functions in ecosystems: Phase matter & scale matter, *Soil Tillage Res.*, 2015, **146**, 1–3.

70 Q. Zhang, G. Liang, D. D. Myrold and W. Zhou, Variable responses of ammonia oxidizers across soil particle-size fractions affect nitrification in a long-term fertilizer experiment, *Soil Biol. Biochem.*, 2017, **105**, 25–36.

71 K. H. Tan, *Humic Matter in Soil and the Environment - Principles and Controversies*, CRC Press, Boca Raton, 2014.

72 G. Giachin, J. Narkiewicz, D. Scaini, A. T. Ngoc, A. Margon, P. Sequi, L. Leita and G. Legname, Prion protein interaction with soil humic substances: Environmental implications, *PLoS One*, 2014, **9**, e100016.

73 K. U. Totsche, W. Amelung, M. H. Gerzabek, G. Guggenberger, E. Klumpp, C. Knief, E. Lehndorff, R. Mikutta, S. Peth, A. Prechtel, N. Ray and I. Kögel-Knabner, Microaggregates in soils, *J. Plant Nutr. Soil Sci.*, 2018, **181**, 104–136.

74 R. R. Weil and N. C. Brady, *The Nature and Properties of Soils*, Pearson Education Limited, Harlow, UK, 15th edn., 2017.

75 D. Ahirwal, A. Hébraud, R. Kádár, M. Wilhelm and G. Schlatter, From self-assembly of electrospun nanofibers to 3D cm thick hierarchical foams, *Soft Matter*, 2013, **9**, 3164.

76 A. Gholipour Kanani and S. H. Bahrami, Effect of Changing Solvents on Poly(-Caprolactone) Nanofibrous Webs Morphology, *J. Nanomater.*, 2011, **2011**, 724153.

77 G. Yang, X. Li, Y. He, J. Ma, G. Ni and S. Zhou, From nano to micro to macro: Electrospun hierarchically structured polymeric fibers for biomedical applications, *Prog. Polym. Sci.*, 2018, **81**, 80–113.

78 E. Bodnár, J. Grifoll and J. Rosell-Llompart, Polymer solution electrospraying: A tool for engineering particles and films with controlled morphology, *J. Aerosol Sci.*, 2018, **125**, 93–118.

79 L. Wang, P. D. Topham, O. O. Mykhaylyk, H. Yu, A. J. Ryan, J. P. A. Fairclough and W. Bras, Self-Assembly-Driven Electrospinning: The Transition from Fibers to Intact Beaded Morphologies, *Macromol. Rapid Commun.*, 2015, **36**, 1437−1443.

80 European Commission, Commission Recommendation of 18 October 2011 on the definition of nanomaterial Text with EEA relevance, http://data.europa.eu/eli/reco/2011/696/oj, (accessed 5 March 2020).

81 J. M. Deitzel, J. Kleinmeyer, D. Harris and N. C. B. Tan, The effect of processing variables on the morphology of electrospun nanofibers and textiles, *Polymer*, 2001, **42**, 261–272.

82 T. Yao, H. Chen, P. Samal, S. Giselbrecht, M. B. Baker and L. Moroni, Self-assembly of electrospun nanofibers into gradient honeycomb structures, *Mater. Des.*, 2019, **168**, 107614.

83 N. Lavielle, A. Hébraud, G. Schlatter, L. Thöny-Meyer, R. M. Rossi and A. M. Popa, Simultaneous electrospinning and electrospraying: A straightforward approach for fabricating hierarchically structured composite membranes, *ACS Appl. Mater. Interfaces*, 2013, **5**, 10090–10097.

84 C. R. Wittmer, A. Hébraud, S. Nedjari and G. Schlatter, Well-organized 3D nanofibrous composite constructs using cooperative effects between electrospinning and electrospraying, *Polymer*, 2014, **55**, 5781–5787.

85 J. Xue, T. Wu, Y. Dai and Y. Xia, Electrospinning and electrospun nanofibers: Methods, materials, and applications, *Chem. Rev.*, 2019, **119**, 5298−5415.

86 I. Jun, H. S. Han, J. R. Edwards and H. Jeon, Electrospun fibrous scaffolds for tissue engineering: Viewpoints on architecture and fabrication, *Int. J. Mol. Sci.*, 2018, **19**, 745.

87 M. Kleber and M. G. Johnson, Advances in Understanding the Molecular Structure of Soil Organic Matter: Implications for Interactions in the Environment, *Adv. Agron.*, 2010, **106**, 77–141.

88 M. Orsi, Molecular dynamics simulation of humic substances, *Chem. Biol. Technol. Agric.*, 2014, **1**, 10.

89 I. Kögel-Knabner and C. Rumpel, Advances in Molecular Approaches for Understanding Soil Organic Matter Composition, Origin, and Turnover: A Historical Overview, *Adv. Agron.*, 2018, **149**, 1–48.

90 V. Guarino, G. Gentile, L. Sorrentino and L. Ambrosio, *Polycaprolactone: Synthesis, Properties, and Applications*, in *Encyclopedia of Polymer Science and Technology*, John Wiley & Sons, Inc., Hoboken, NJ, USA, 2017, pp. 1–36.

91 P. Roach, N. J. Shirtcliffe and M. I. Newton, Progess in superhydrophobic surface development, *Soft Matter*, 2008, **4**, 224–240.

92 W. M. Dunne, Bacterial adhesion: Seen any good biofilms lately?, *Clin. Microbiol. Rev.*, 2002, **15**, 155–166.

93 H. Dang and C. R. Lovell, Microbial Surface Colonization and Biofilm Development in Marine Environments, *Microbiol. Mol. Biol. Rev.*, 2016, **80**, 91–138.

94 C. Beloin, A. Roux and J. M. Ghigo, *Escherichia coli* biofilms, *Curr. Top. Microbiol. Immunol.*, 2008, **322**, 249–289.

95 M. Katsikogianni and Y. F. Missirlis, Concise review of mechanisms of bacterial adhesion to biomaterials and of techniques used in estimating bacteria-material interactions, *Eur. Cells Mater.*, 2004, **8**, 37–57.

96 G. Li, L.-K. Tam and J. X. Tang, Amplified effect of Brownian motion in bacterial near-surface swimming, *Proc. Natl. Acad. Sci.*, 2008, **105**, 18355–18359.

97 R. D. Monds and G. A. O'Toole, The developmental model of microbial biofilms: ten years of a paradigm up for review., *Trends Microbiol.*, 2009, **17**, 73–87.

98 L. G. Ribba, J. D. Cimadoro, N. B. D'Accorso and S. N. Goyanes, *Removal of Pollutants Using Electrospun Nanofiber Membranes*, in *Industrial Applications of Renewable Biomass Products: Past, Present and Future*, eds. S. N. Goyanes and N. B. D'Accorso, Springer International Publishing AG, 2017, pp. 1–332.

99 M. Kargar, J. Wang, A. S. Nain and B. Behkam, Controlling bacterial adhesion to surfaces using topographical cues: a study of the interaction of *Pseudomonas aeruginosa* with nanofiber-textured surfaces, *Soft Matter*, 2012, **8**, 10254.

100 M. Abrigo, P. Kingshott and S. L. McArthur, Electrospun polystyrene fiber diameter influencing bacterial attachment, proliferation, and growth, *ACS Appl. Mater. Interfaces*, 2015, **7**, 7644–7652.

101 K. A. Rieger, R. Thyagarajan, M. E. Hoen, H. F. Yeung, D. M. Ford and J. D. Schiffman, Transport of microorganisms into cellulose nanofiber mats, *RSC Adv.*, 2016, **6**, 24438–24445.

102 C. Rumbo, J. A. Tamayo-Ramos, M. F. Caso, A. Rinaldi, L. Romero-Santacreu, R. Quesada and S. Cuesta-López, Colonization of electrospun polycaprolactone fibers by relevant pathogenic bacterial strains, *ACS Appl. Mater. Interfaces*, 2018, **10**, 11467–11473.

103 J. A. Tamayo-Ramos, C. Rumbo, F. Caso, A. Rinaldi, S. Garroni, A. Notargiacomo, L. Romero-Santacreu and S. Cuesta-López, Analysis of Polycaprolactone Microfibers as Biofilm Carriers for Biotechnologically Relevant Bacteria, *ACS Appl. Mater. Interfaces*, 2018, **10**, 32773–32781.

104 J. Geng and N. Henry, *Short Time-Scale Bacterial Adhesion Dynamics*, in *Bacterial Adhesion: Chemistry, Biology and Physics*, Springer, Dordrecht, 2011, pp. 315–331.

105 N. Siboni, M. Lidor, E. Kramarsky-Winter and A. Kushmaro, Conditioning film and initial biofilm formation on ceramics tiles in the marine environment, *FEMS Microbiol. Lett.*, 2007, **274**, 24–29.

106 A. Garg, A. Jain and N. B. Bhosle, Chemical characterization of a marine conditioning film, *Int. Biodeterior. Biodegrad.*, 2009, **63**, 7–11.

107 A. E. Scott, M. N. Burtnick, M. G. M. Stokes, A. O. Whelan, E. D. Williamson, T. P. Atkins, J. L. Prior and P. J. Brett, *Burkholderia pseudomallei* Capsular Polysaccharide Conjugates Provide Protection against Acute Melioidosis, *Infect. Immun.*, 2014, **82**, 3206–3213.

108 A. E. Essex-Lopresti, J. A. Boddey, R. Thomas, M. P. Smith, M. G. Hartley, T. Atkins, N. F. Brown, C. H. Tsang, I. R. A. Peak, J. Hill, I. R. Beacham and R. W. Titball, A type IV pilin, pilA, contributes to adherence of *Burkholderia pseudomallei* and virulence in vivo, *Infect. Immun.*, 2005, **73**, 1260–1264.

109 V. Pelicic, Type IV pili: e pluribus unum?, *Mol. Microbiol.*, 2008, **68**, 827–837.

110 L. L. Burrows, *Pseudomonas aeruginosa* twitching motility: type IV pili in action., *Annu. Rev. Microbiol.*, 2012, **66**, 493–520.

111 L. Craig, K. T. Forest and B. Maier, Type IV pili: dynamics, biophysics and functional consequences, *Nat. Rev. Microbiol.*, 2019, **17**, 429–440.

112 L. Craig, M. E. Pique and J. A. Tainer, Type IV pilus structure and bacterial pathogenicity, *Nat. Rev. Microbiol.*, 2004, **2**, 363–378.

113 J. S. Mattick, Type IV Pili and Twitching Motility, *Annu. Rev. Microbiol.*, 2002, **56**, 289–314.

114 R. Zhang, J. J. LiPuma and C. F. Gonzalez, Two type IV secretion systems with different functions in *Burkholderia cenocepacia* K56-2, *Microbiology*, 2009, **155**, 4005–4013.

115 S. Ganesan and U. S. Sajjan, Host Evasion by *Burkholderia cenocepacia*, *Front. Cell. Infect. Microbiol.*, 2012, **1**, 25.

116 S. Burdman, O. Bahar, J. K. Parker and L. de la Fuente, Involvement of type IV pili in pathogenicity of plant pathogenic bacteria, *Genes (Basel).*, 2011, **2**, 706–735.

117 N. R. Luke, A. J. Howlett, J. Shao and A. A. Campagnari, Expression of Type IV Pili by *Moraxella catarrhalis* Is Essential for Natural Competence and Is Affected by Iron Limitation, *Infect. Immun.*, 2004, **72**, 6262–6270.

118 M. Tomich and C. D. Mohr, Adherence and autoaggregation phenotypes of a *Burkholderia cenocepacia* cable pilus mutant, *FEMS Microbiol. Lett.*, 2003, **228**, 287–297.

119 A. T. Jan, Outer Membrane Vesicles (OMVs) of gram-negative bacteria: A perspective update, *Front. Microbiol.*, 2017, **8**, 1053.

120 C. Florez, J. E. Raab, A. C. Cooke and J. W. Schertzer, Membrane distribution of the *Pseudomonas* quinolone signal modulates outer membrane vesicle production in *Pseudomonas aeruginosa*, *MBio*, 2017, **8**, e01034-17.

121 M. E. Anyan, A. Amiri, C. W. Harvey, G. Tierra, N. Morales-Soto, C. M. Driscoll, M. S. Alber and J. D. Shrout, Type IV pili interactions promote intercellular association and moderate swarming of *Pseudomonas aeruginosa*, *Proc. Natl. Acad. Sci. U. S. A.*, 2014, **111**, 18013–18018.

122 E. Grohmann, P. J. Christie, G. Waksman and S. Backert, Type IV secretion in Gram-negative and Gram-positive bacteria, *Mol. Microbiol.*, 2018, **107**, 455–471.

123 S. Vadia and P. A. Levin, Growth rate and cell size: A re-examination of the growth law, *Curr. Opin. Microbiol.*, 2015, **24**, 96–103.

124 C. R. Armbruster, C. K. Lee, J. Parker-Gilham, J. De Anda, A. Xia, K. Zhao, K. Murakami, B. S. Tseng, L. R. Hoffman, F. Jin, C. S. Harwood, G. C. L. Wong and M. R. Parsek,

Heterogeneity in surface sensing suggests a division of labor in *Pseudomonas aeruginosa* populations, *Elife*, 2019, **8**, e45084.

125 M. M. E. Metruccio, D. J. Evans, M. M. Gabriel, J. L. Kadurugamuwa and S. M. J. Fleiszig, *Pseudomonas aeruginosa* outer membrane vesicles triggered by human mucosal fluid and lysozyme can prime host tissue surfaces for bacterial adhesion, *Front. Microbiol.*, 2016, **7**, 871.

126 A. Kulp and M. J. Kuehn, Biological functions and biogenesis of secreted bacterial outer membrane vesicles, *Annu. Rev. Microbiol.*, 2010, **64**, 163–184.

127 N. Couto, S. R. Schooling, J. R. Dutcher and J. Barber, Proteome Profiles of Outer Membrane Vesicles and Extracellular Matrix of Pseudomonas aeruginosa Biofilms, *J. Proteome Res.*, 2015, **14**, 4207–4222.

128 M. E. Davey, N. C. Caiazza and G. A. O'Toole, Rhamnolipid surfactant production affects biofilm architecture in *Pseudomonas aeruginosa* PAO1, *J. Bacteriol.*, 2003, **185**, 1027–1036.

129 J. D. Shrout, D. L. Chopp, C. L. Just, M. Hentzer, M. Givskov and M. R. Parsek, The impact of quorum sensing and swarming motility on *Pseudomonas aeruginosa* biofilm formation is nutritionally conditional, *Mol. Microbiol.*, 2006, **62**, 1264–1277.

130 C. Wang, W. Chen, A. Xia, R. Zhang, Y. Huang, S. Yang, L. Ni and F. Jin, Carbon Starvation Induces the Expression of PprB-Regulated Genes in *Pseudomonas aeruginosa*, *Appl. Environ. Microbiol.*, 2019, **85**, e01705-19.

131 S. Biswas, P. Mukherjee, T. Manna, K. Dutta, K. C. Guchhait, A. Karmakar, M. Karmakar, P. Dua, A. K. Panda and C. Ghosh, Quorum Sensing Autoinducer(s) and Flagellum Independently Mediate EPS Signaling in Vibrio cholerae Through LuxO-Independent Mechanism, *Microb. Ecol.*, 2019, **77**, 616–630.

132 J. Zhang and C. L. Poh, Regulating exopolysaccharide gene wcaF allows control of Escherichia coli biofilm formation, *Sci. Rep.*, 2018, **8**, 13127.

133 H. C. Flemming and J. Wingender, The biofilm matrix, *Nat. Rev. Microbiol.*, 2010, **8**, 623–633.

134 M. V. Zhurina, A. V. Gannesen, E. L. Zdorovenko and V. K. Plakunov, Composition and functions of the extracellular polymer matrix of bacterial biofilms, *Microbiology*, 2014, **83**, 713–722.

135 H.-C. Flemming, EPS-Then and Now, *Microorganisms*, 2016, **4**, 41.

136 V. J. M. Allan, M. E. Callow, L. E. Macaskie and M. Paterson-Beedle, Effect of nutrient limitation on biofilm formation and phosphatase activity of a Citrobacter sp., *Microbiology*, 2002, **148**, 277–288.

137 N. R. Stanley and B. A. Lazazzera, Environmental signals and regulatory pathways that influence biofilm formation, *Mol. Microbiol.*, 2004, **52**, 917–924.

138 I. L. Pepper and T. J. Gentry, *Earth Environments*, in *Environmental Microbiology*, Academic Press, Third Edit., 2015, pp. 59–88.

139 Y. Kuzyakov and E. Blagodatskaya, Microbial hotspots and hot moments in soil: Concept & review, *Soil Biol. Biochem.*, 2015, **83**, 184–199.

140 N. S. Bolan, D. C. Adriano, A. Kunhikrishnan, T. James, R. McDowell and N. Senesi, Dissolved Organic Matter. Biogeochemistry, Dynamics, and Environmental Significance in Soils., *Adv. Agron.*, 2011, **110**, 1–75.

141 M. Borisover, A. Lordian and G. J. Levy, Water-extractable soil organic matter characterization by chromophoric indicators: Effects of soil type and irrigation water quality, *Geoderma*, 2012, **179–180**, 28–37.

142 A. L. Mills, Keeping in Touch: Microbial Life on Soil Particle Surfaces, *Adv. Agron.*, 2003, **78**, 1–43.

143 C. Chenu and G. Stotzky, *Interactions between Microorganisms and Soil Particles: An Overview*, in *Interactions Between Soil Particles and Microorganisms*, eds. P. M. Huang, J.-M. Bollag and N. Senesi, John Wiley and Sons, Ltd., 2002, pp. 3–40.

View Article Online
DOI: 10.1039/D0EN00268B

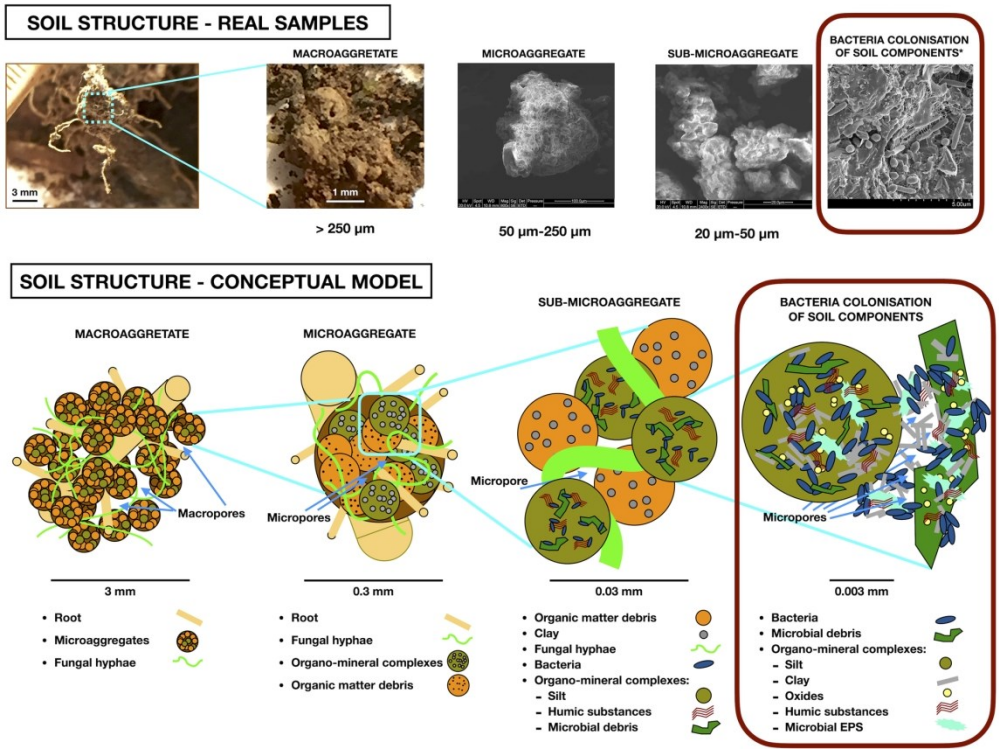

Sketch of different levels of soil particle aggregations and participated organisms (mostly microorganisms and roots) resulting in the soil structure. The level that the present study aimed at mimicking is highlighted by dark red rectangles. *Image courtesy of the Lewis Lab at Northeastern University. Image created by Anthony D'Onofrio, William H. Fowle, Eric J. Stewart and Kim Lewis.

170x128mm (300 x 300 DPI)

View Article Online
DOI: 10.1039/D0EN00268B

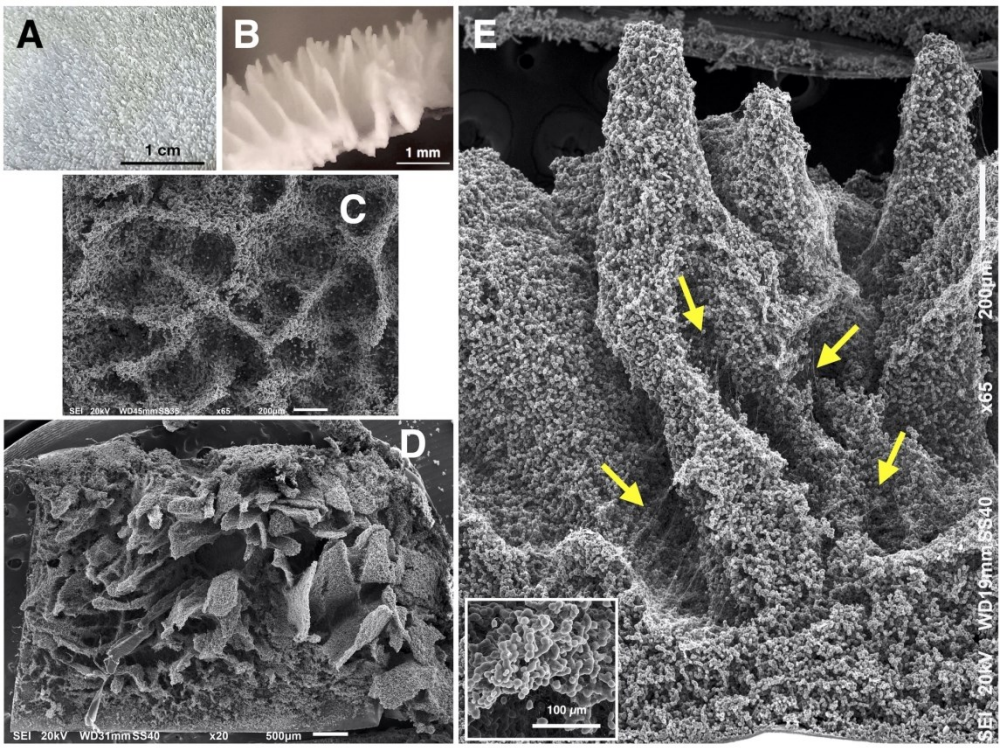

Figure 2. Optical images and SEM micrographs of the pristine Electrospun Nanostructured (beads-and-fibres) PCL Scaffold-1 (*EN-PCLS$_1$*). (A) Optical images of the *EN-PCLS$_1$*, top view. (B) Optical images of the *EN-PCLS$_1$*, lateral view. (C) SEM micrograph (65X magnification) of the thin area displaying the honeycomb wax cell-like arrangement, top view. (D) SEM micrograph of the thick zone displaying the flakes and pinnacles arising from the honeycomb wax cell-like arrangement, top view. (E) SEM micrograph of the cross-section of the thick zone displaying details of the beads-and-fibre framework of the flakes and pinnacles corresponding to upward extensions of the honeycomb wax cell-like walls with the relative cavities appearing as channels or trenches where fibres are more evident (yellow arrows); inset = detail of the microbeads from the walls (pinnacles) of the honeycomb wax cell-like arrangement often appearing as fused. Scale bars: (A) = 1 cm; (B) 1 mm; (C) = 200 µm; (D) = 500 µm; (E) = 200 µm (inset = 100 µm).

170x128mm (300 x 300 DPI)

View Article Online
DOI: 10.1039/D0EN00268B

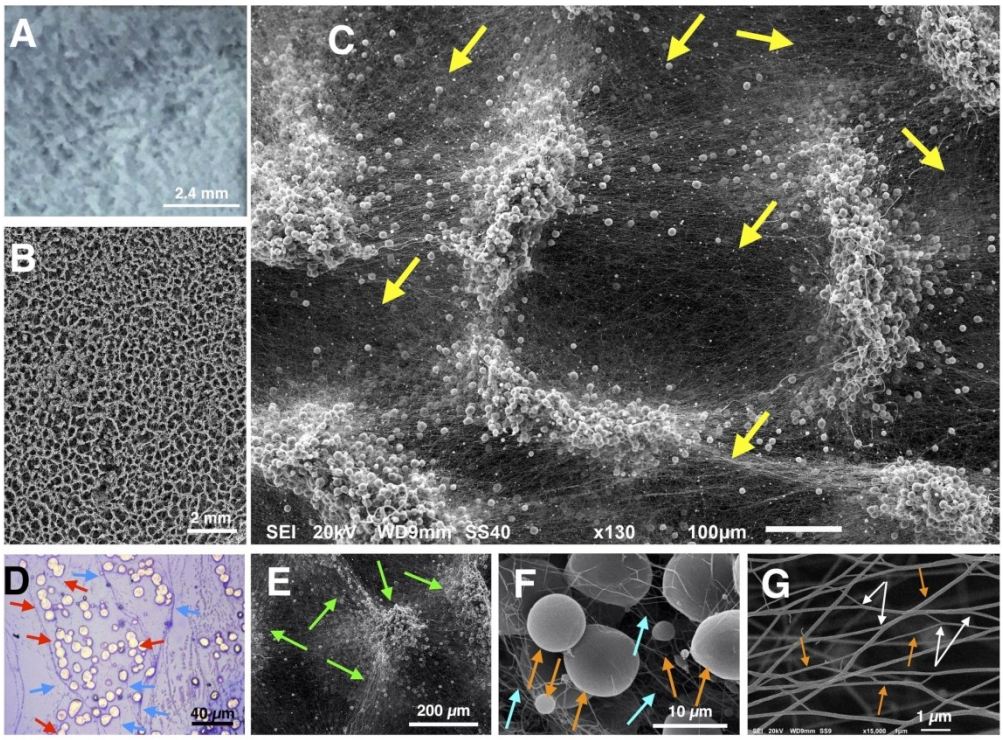

Figure 3. Optical images and SEM micrographs of the pristine Electrospun Nanostructured (beads-and-fibres) PCL Scaffold-2 (*EN-PCLS$_2$*). (A, B) Honeycomb wax cell-like arrangement of the mat, top view optical microscopy and SEM, respectively. (C) SEM micrograph displaying the top view of the honeycomb wax cell-like arrangement deriving from the beads-and-fibre deposition by electrospinning (D) Light microscope image of the cross-section of the beads-and-fibres framework (*red* and *light blue arrows*, respectively). (E) SEM micrograph displaying the walls of the honeycomb wax cell-like arrangement upon electrospinning prevalently composed of microbeads (*green arrows*). (F) SEM micrograph displaying in detail the dimensional proportions between microbeads (*orange arrows*) and nanofibres (*pale blue arrows*) comprising the electrospun fabric. (G) SEM micrograph displaying in detail the nanofibres comprising the electrospun fabric; *orange arrows* = single nanofibres; *white arrows* = split nanofibres. Scale bars: (A) = 2.4 mm; (B) 2 mm; (C) = 100 µm; (D) = 40 µm; (E) = 200 µm; (F) = 10 µm; (G) = 1 µm.

170x128mm (300 x 300 DPI)

View Article Online
DOI: 10.1039/D0EN00268B

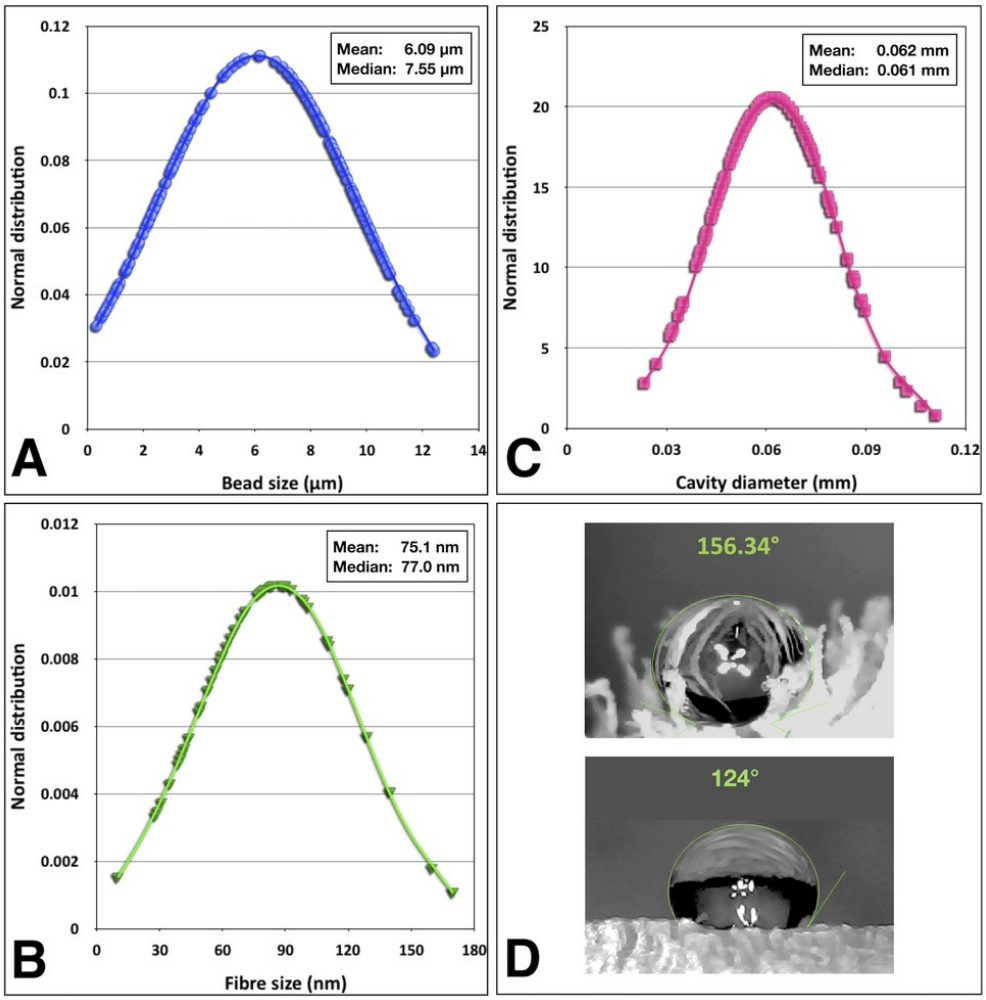

Figure 4. Characterisation of the Electrospun Nanostructured PCL Scaffolds (*EN-PCLSs*): A) Distribution of the diameters of beads in the pristine *EN-PCLS*$_2$ upon deposition. (B) Distribution of the diameters of fibres in the pristine *EN-PCLS*$_2$ upon deposition. (C) Distribution of the diameters of cavities in the honeycomb wax cell-like arrangement of the pristine *EN-PCLS*$_2$ upon deposition and 3 h incubation with bacteria. D) The contact angle of *EN-PCLSs* (drop volume = 8 µl and 7 µl for *EN-PCLS*$_1$ and *EN-PCLS*$_2$, respectively). The sizes of distinct structures (beads, fibres and cavities) of *EN-PCLS*$_2$ were measured in SEM micrographs of the nanoframeworks (n = 220 (A); n = 145 (B); n = 135 (C)). Means and median values of the structures are displayed within the relative plots.

82x83mm (300 x 300 DPI)

View Article Online
DOI: 10.1039/D0EN00268B

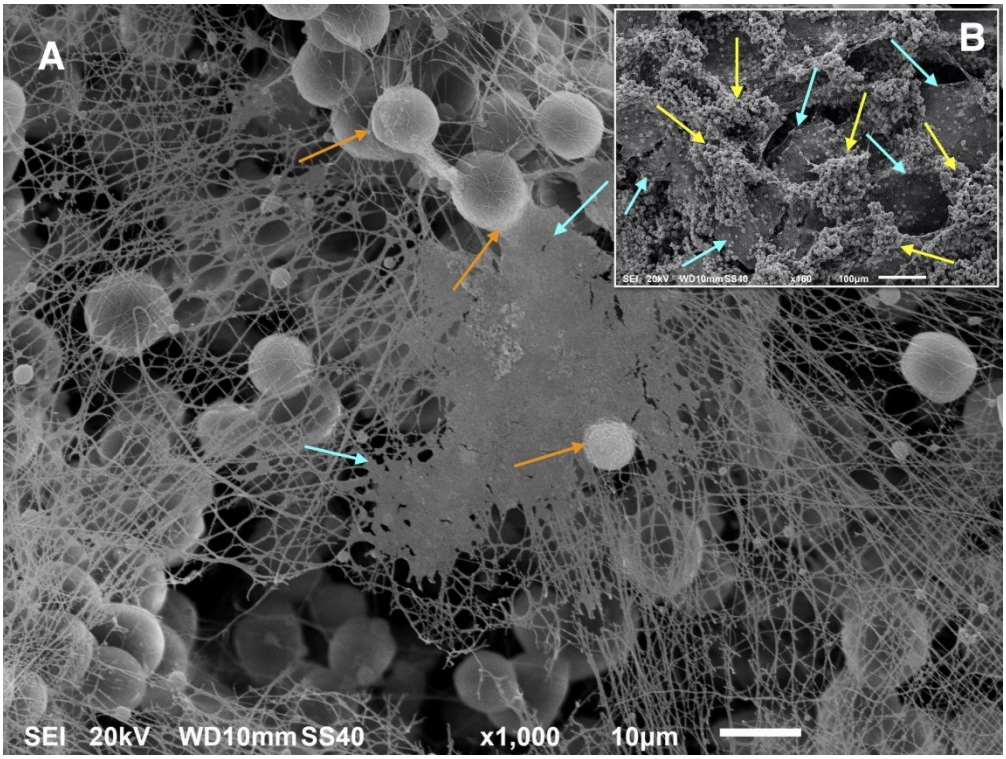

Figure 5. SEM micrographs of *EN-PCLSs* after 3 h incubation in the *B. terricola* cells suspension: (A) conditioning film (CF) forming membranes upon its deposition by bacteria on the nanofibrous network within the cavities but close to the walls of the honeycomb wax cell-like structures (*pale blue arrows*); *orange arrows* = microbeads appearing covered with CF. (B) Massive deposition of CF in the nanofibrous cavities of honeycomb wax cell-like structures (*pale blue arrows*); *yellow arrows* = aggregates of microbeads appearing as protruding from this coating. Scale bars: (A) = 10 µm; (B) 100 µm.

170x128mm (300 x 300 DPI)

View Article Online
DOI: 10.1039/D0EN00268B

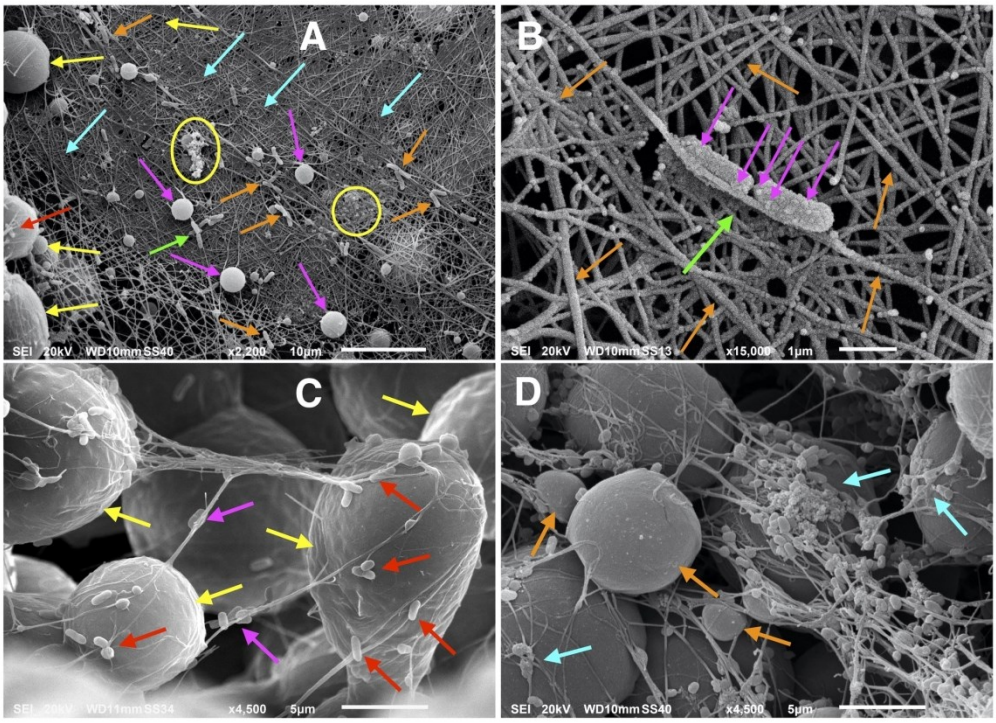

Figure 6. SEM micrographs highlighting evidences that *B. terricola* cells attached prevalently to the nanofibres of *EN-PCLSs* during the incubation. (A) Bacteria starting adhering after 5 h incubation to the nanoframework close to the wall of a cavity of the honeycomb wax cell-like arrangement; *pale blue arrows* = conditioning film (CF) forming membranes on the nanofibrous network within the cavities of the honeycomb wax cell-like structures after 5 h incubation upon its deposition by bacteria; *yellow* and *pink arrows* = aggregates of microbeads in the walls of the honeycomb wax cell-like structure and single microbeads entrapped in the nanofibrous network, respectively, showing no bacteria adhering on them; *orange* and *red arrows* = *B. terricola* cells attached to the nanofibres in the cavity and on a microbead, respectively; *yellow circles* = outer membrane vesicles (OMV) spread on the nanofibres and grouped in clusters; (B) Interactions of *B. terricola* cells and nanofibres at early stages of incubation (5 h); *pink arrows* = i) very close interaction between bacteria cells and the nanofibres pointing out the very different size between these two components, ii) polymeric matrix surrounding bacteria cells and wrapping the CF-coated nanofibres, and iii) OMVs attached to the bacterial surfaces and at the interfaces; *orange arrows* = larger size of nanofibres upon CF deposition. (C) Interactions of *B. terricola* cells and microbeads at early stages of incubation (5 h); *red arrows* = bacteria cells adhering to the microbeads only where the nanofibres are present; *pink arrows* = bacteria cells hanging on the nanofibres; *yellow arrows* = CF coating the microbeads. (D) Interactions of *B. terricola* cells and microbeads after 48 h incubation; *pale blue arrows* = bacteria adhering to microbeads provided the latter were coated with nanofibres; *orange arrows* = bacteria-free microbeads in the absence of nanofibres deposited on them. Scale bars: (A) = 10 µm; (B) 1 µm; (C) and (D) = 5 µm.

170x128mm (300 x 300 DPI)

View Article Online
DOI: 10.1039/D0EN00268B

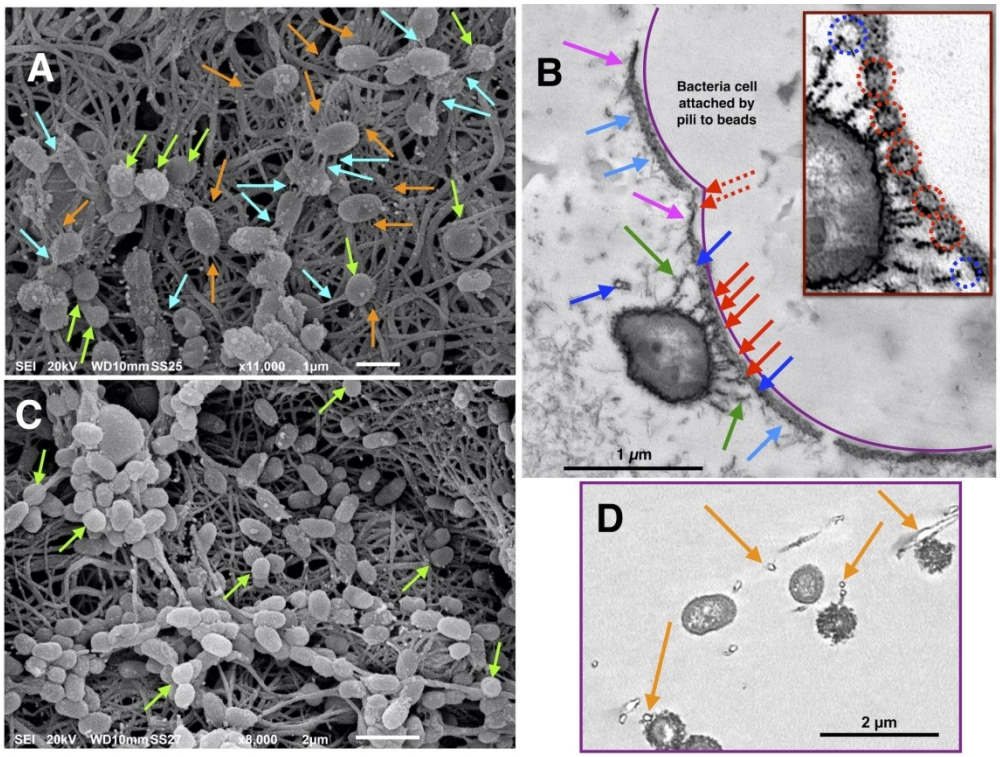

Figure 7. Stable attachment of *B. terricola* cells to *EN-PCLSs*: (A) SEM micrograph highlighting evidences that after 28 h incubation *B. terricola* cells started forming appendages protruding throughout their surfaces following a radial distribution to anchor to the nanofibrous network (*orange arrows*) and to link each other (*light blue arrows*); *green arrows* = *B. terricola* cells showing spherical shapes (the other cells are displaying egg-shaped morphology). (B) TEM micrographs of a *B. terricola* cell adhering to a microbead: *green arrows* = bacterial appendages enabling the attachment of the cell to the microbead; *light blue arrows* = CF deposited onto the microbead; *pink arrows* = microbial surface deprived of CF; *red arrows* = vesicles apparently linking microbial appendages to the CF-coated microbead surface (*solid arrows*) or free on the microbead surface (*dotted arrow*); inset = cross-sections of electron-dense and bright core vesicles (d*dotted red* and *blue rings*, respectively). (C) SEM micrograph of *B. terricola* cells showing spherical (*green arrows*) and egg-shaped morphology after 48 h incubation. (D) TEM micrographs of *B. terricola* cell after 28 h incubation interacting directly, in some cases, with nanofibres, here often appearing as transversal and longitudinal sections (*orange arrows*). Scale bars: (A) and (B) = 1 µm; (C) and (D) = 2 µm.

170x128mm (300 x 300 DPI)

View Article Online
DOI: 10.1039/D0EN00268B

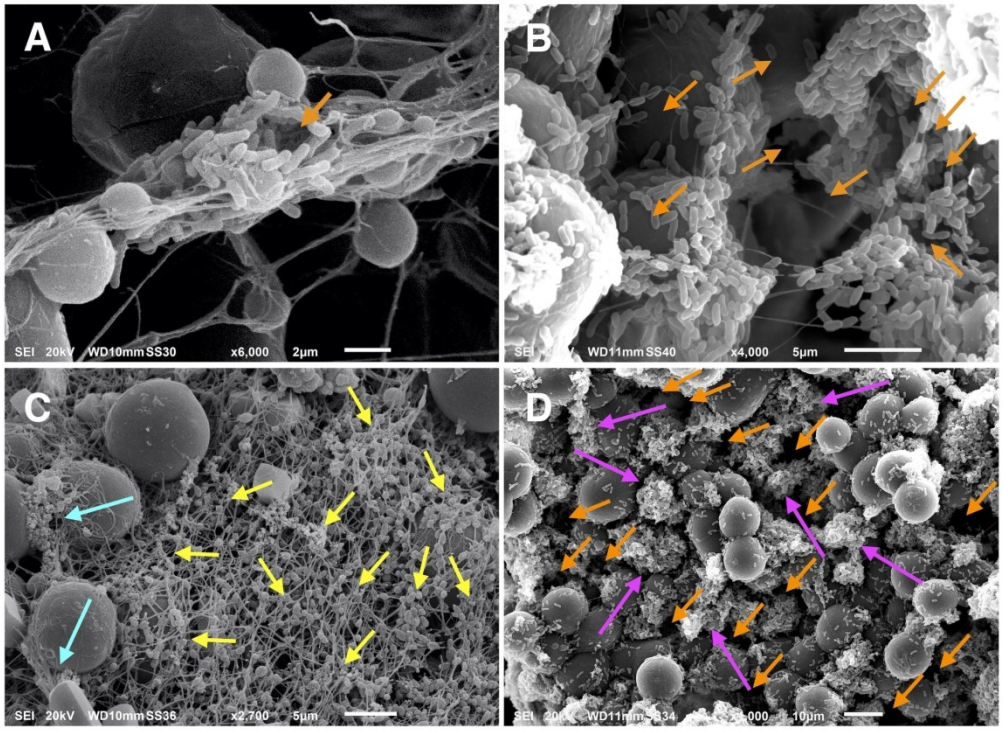

Figure 8. SEM micrographs of the colonisation of *EN-PCLSs* by *B. terricola* cells after 5 h to 28 h incubation: (A) Development after 5 h incubation of microcolonies of rod-like cells hung on suspended nanofibres in the honeycomb structure. (B) Bacterial microcolonies after an incubation period of 20 h displaying preferential growth and enlargement on the tiny nanofibres of *EN-PCLSs*; *orange arrows* = holes crossing the colonies. (C) Extensive colonisation of *EN-PCLSs* by *B. terricola* cells observed after 28 h incubation: the area displayed is close to the wall of a cavity of the honeycomb wax cell-like arrangement; *yellow arrows*= colonisation of the nanofibrous network of the cavity; *pale blue arrows* = colonisation of the spaces between the microbeads in the presence of the nanofibrous network. (D) 3D microcolonies of *B. terricola* cells sited prevalently in the spaces between the microbeads (*pink arrows*) after 28 h incubation; *orange arrows* = holes crossing the colonies. Scale bars: (A) = 2; (B) and (C) = 5 µm; (D) = 10 µm.

170x128mm (300 x 300 DPI)

View Article Online
DOI: 10.1039/D0EN00268B

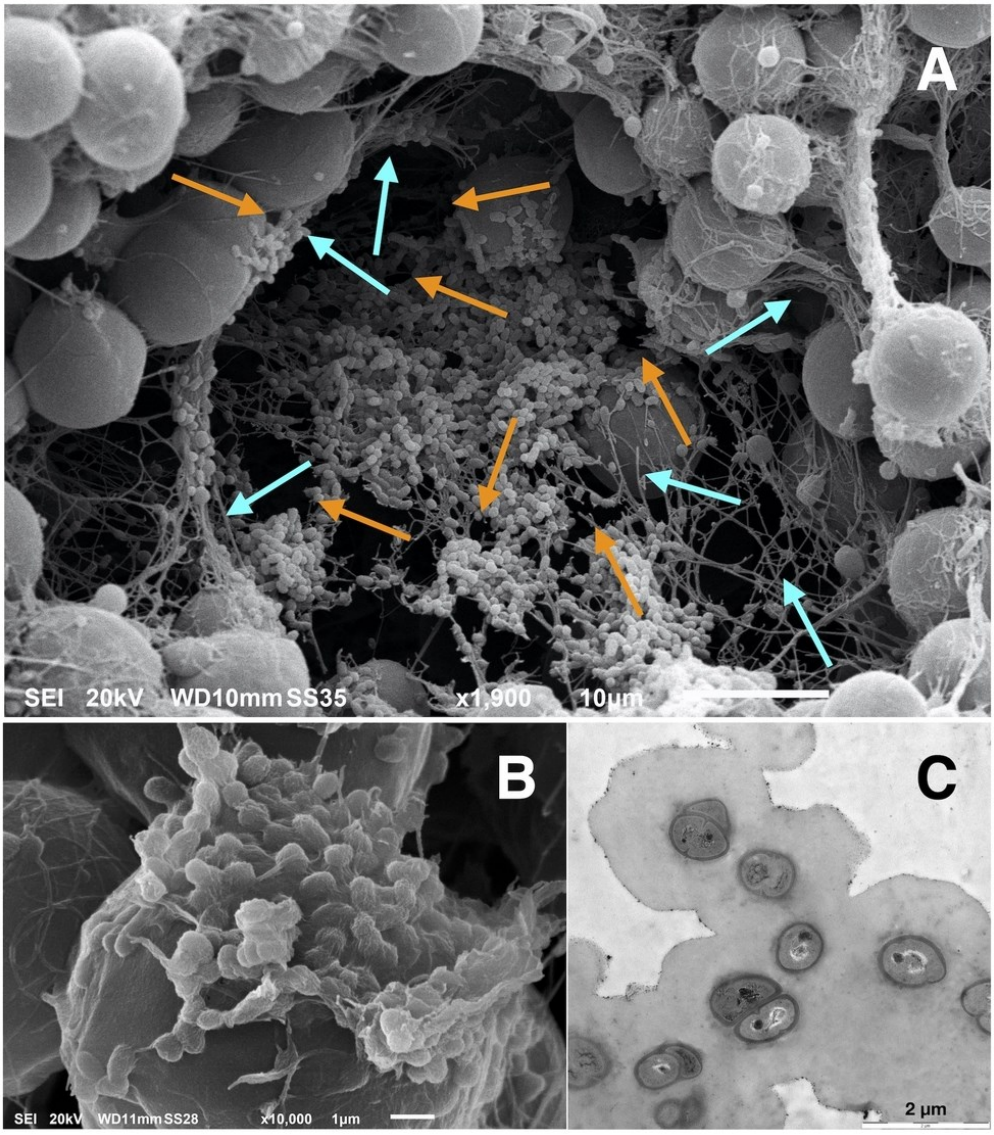

Figure 9. SEM and TEM micrographs of the colonisation of *EN-PCLSs* by *B. terricola* cells after 48 h incubation: (A) SEM micrograph of a 3D macrocolony of *B. terricola* cells sited preferentially in the vast space between microbead aggregates, provided that a nanofibrous network was present; *pale blue arrows* = nanofibrous network as a support enabling the macrocolony formation; *orange arrows* = holes crossing the colonies. (B) SEM micrograph displaying EPS release and its involvement in the formation of stable interactions between bacteria and of them with the *EN-PCLSs* upon progressive envelopment and embedment of bacteria cells by such matrix. (C) TEM micrographs showing bacterial cells surrounded by EPS, which appeared here as a dark halo around the cells. Scale bars: (A) = 10; (B) = 1 µm; (C) = 2 µm.

82x94mm (300 x 300 DPI)

View Article Online
DOI: 10.1039/D0EN00268B

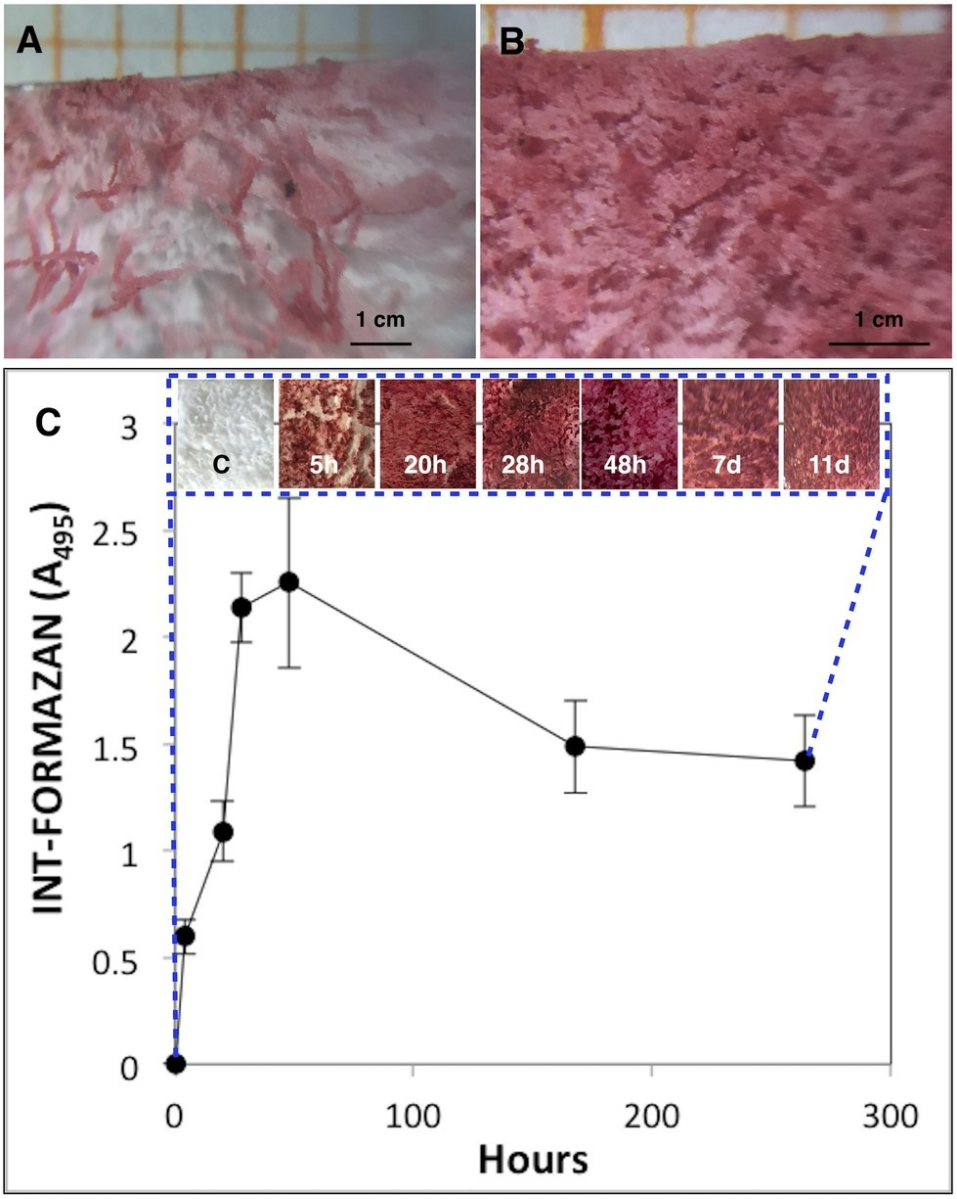

Figure 10. Measurement of the vital and metabolically active *B. terricola* cells by INT reduction to its formazan during the biofilm development on the nanostructured PCL fabrics SEM. (A) and (B) Pictures of *EN-PCLSs* displaying the variation and distribution of the red colour due to the more significant reduction of INT to its formazan and related to changes of the extent of bacteria in the colonised nanostructured fabrics and of bacteria diffusion through them: (A) Colonisation of the *EN-PCLSs* occurring at first at the borders of the mats; (B) Colonisation proceeding inwards until spreading throughout the nanoframeworks. (C) Dynamics of bacterial population growth during the incubation period (11 d) based on absorbance at 495 nm of the formazan extracted from *EN-PCLSs* and then normalised to the size of the *EN-PCLSs* (namely 1 mm2); insets = Pictures displaying the extent of INT-formazan on *EN-PCLSs* sampled at various incubation periods and related to the growth and metabolic activity of the bacterial populations on the mats.

82x103mm (300 x 300 DPI)

View Article Online
DOI: 10.1039/D0EN00268B

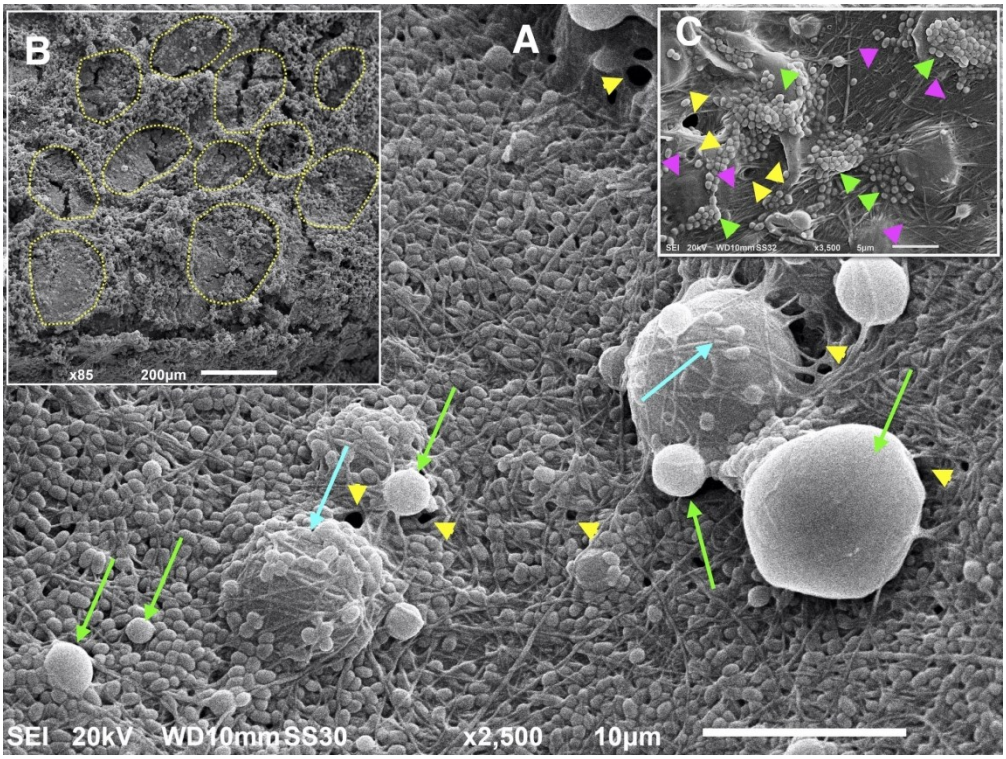

Figure 11. SEM micrographs of *B. terricola* biofilms developed on the *EN-PCLSs* after 7d incubation (*BEN-PCLSs*). (A) A layer of densely packed bacteria embedded in the EPS matrix globally forming a uniform coating covering the *EN-PCLSs*, and thus generating a young biofilm (*BEN-PCLSs*); *green arrows* = microbeads without deposited nanofibres still appearing free of bacteria on them; *yellow arrowheads* = holes crossing the colonies; *pale blue arrows* = microbeads with nanofibres on their surfaces housing bacteria depending on the number of the nanofibres deposited. (B) Overview of the *BEN-PCLSs*showing that, at this stage of the microbial community evolution, the original honeycomb wax cell-like architecture of the nanostructured fabrics was hardly identifiable (Fig. 11b, *dotted yellow circles*), because of the considerable bacterial population and the extensive presence of the EPS coating. (C) Overview of the mature biofilm developed on the *BEN-PCLSs*, where EPS formed a thick matrix embedding both the bacteria cells and the nanofibrous frameworks that finally appearing like a blanket coating the mats (*pink arrowheads*); *green arrowheads* = bacterial colonies protruding from the EPS matrix; *yellow arrowheads* = holes crossing the colonies. Scale bars: (A) = 10; (B) = 200 µm; (C) = 5 µm.

170x128mm (300 x 300 DPI)

View Article Online
DOI: 10.1039/D0EN00268B

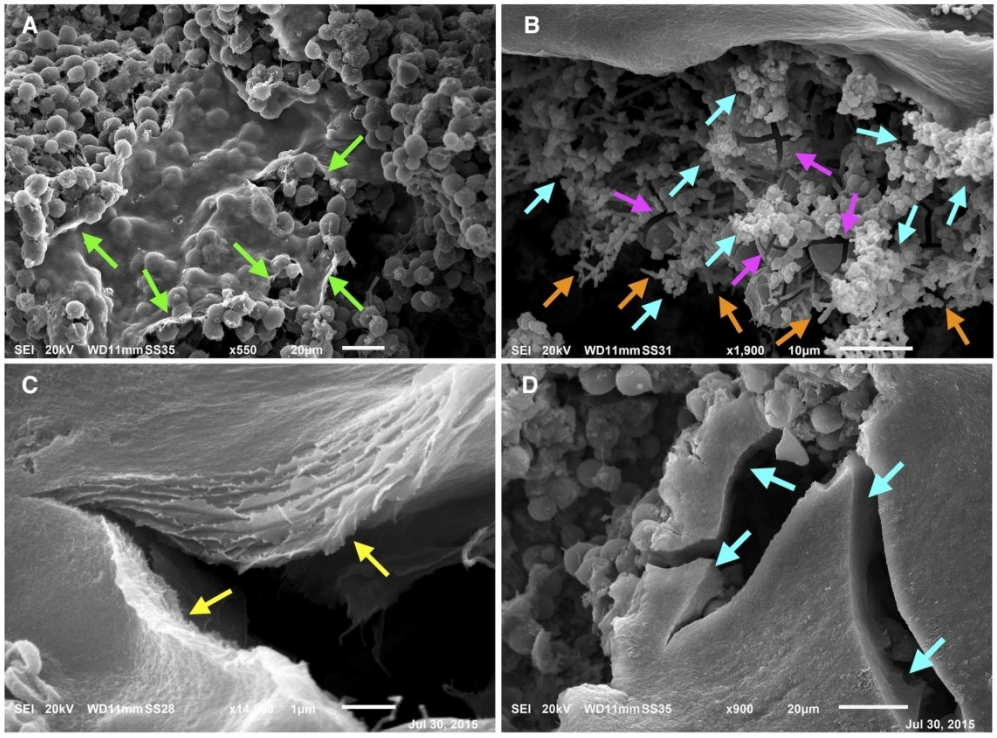

Figure 12. SEM micrographs showing the degradation of the biofilm generated by *B. terricola* cells on *EN-PCLSs* after 11 d incubation. (A) Partial degradation of the EPS coating covering the *BEN-PCLSs* highlighted by extensive rips (*green arrows*); (B) Degradation of the bacteria-colonised nanoframeworks beneath the top EPS coating displaying the break down of both the microbeads (*pink arrows*) and the fibrous network (*orange arrows*) supporting the bacterial colonies (*pale blue arrows*). (C) Multilayered organisation of the EPS coating covering *BEN-PCLSs* as it appears where lacerations occurs (*yellow arrows*). (D) The thickness of the EPS coating as visible from the cracks induced by degradation (*pale blue arrows*). Scale bars: (A) = 20; (B) = 10 µm; (C) = 1 µm; (D) = 20 µm.

170x128mm (300 x 300 DPI)

View Article Online
DOI: 10.1039/D0EN00268B

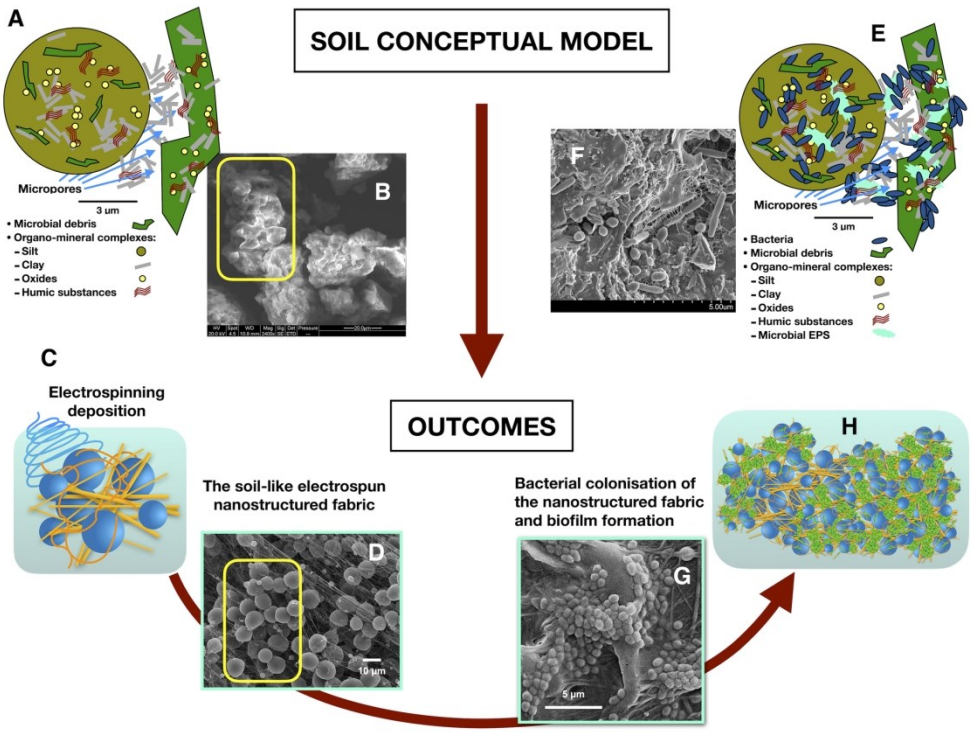

Diagram comparing the aims fixed in the present study, i.e. the creation of 3D nanostructured fabrics mimicking the 3D soil architecture at the microscale and nanoscale level in order to be more "naturally" colonised by bacteria until forming proper mature biofilms, and the relative outcomes. (A) Sketch of the soil conceptual model as composed of aggregates of various solid particles (silt, clay and oxides) and organic matter (microbial debris and humic substances), and 3D image of natural soil aggregates at the microscale (B). The components in the sketch have been reproduced respecting the relative average sizes. The yellow rectangle in (B) points out a typical soil micraggregate. (C) Sketch of a 3D electrospun nanostructured framework (*EN-PCLSs*) here fabricated and composed of beads and fibres to reproduce the solid particles and the fibrous organic matter of the real soil, respectively, and image of the real *EN-PCLSs* generated (D). The *yellow rectangle* in (D) highlights the presence of aggregates of microbeads and fibrous organic material with similar dimensions as in (B). (E) Sketch of a soil aggregate as in (A) colonised by bacteria, and 3D image of a natural soil microaggregate colonised by biofilm-forming bacteria (F). (H) Sketch of the *EN-PCLSs* here fabricated when colonised by bacteria, and image of an *EN-PCLS* colonised by bacteria after the development of a mature biofilm (G). (F) Image courtesy of the Lewis Lab at Northeastern University. Image created by Anthony D'Onofrio, William H. Fowle, Eric J. Stewart and Kim Lewis.

170x128mm (300 x 300 DPI)

TABLE OF CONTENTS (TOC) - CAPTION

View Article Online
DOI: 10.1039/D0EN00268B

Creation of beads-and-fibres 3D nanoscaffolds mimicking the typical architecture of soils at microscale and nanoscale for the development of bacterial biofilms for agricultural and environmental applications.

View Article Online
DOI: 10.1039/D0EN00268B